Available online at www.sciencedirect.com

SCIENCE DIRECT®

Lithos 86 (2006) 281–302

LITHOS

www.elsevier.com/locate/lithos

Early Cretaceous gabbroic rocks from the Taihang Mountains: Implications for a paleosubduction-related lithospheric mantle beneath the central North China Craton

Yuejun Wang [a,*], Weiming Fan [a], Hongfu Zhang [b], Touping Peng [a]

[a] *Key Laboratory of Isotope Geochronology and Geochemistry, Guangzhou Institute of Geochemistry, Chinese Academy of Sciences, P.O. Box 1131, Guangzhou 510640, China*

[b] *State Key Laboratory of Lithosphere Tectonic Evolution, Institute of Geology and Geophysics, Chinese Academy of Sciences, Beijing 100029, China*

Received 9 June 2004; accepted 18 July 2005
Available online 22 August 2005

Abstract

SHRIMP zircon U–Pb ages and geochemical and Sr–Nd–Pb isotopic data are presented for the gabbroic intrusive from the southern Taihang Mountains to characterize the nature of the Mesozoic lithospheric mantle beneath the central North China Craton (NCC). The gabbroic rocks emplaced at 125 Ma and are composed of plagioclase (40–50%), amphibole (20–30%), clinopyroxene (10–15%), olivine (5–10%) and biotite (5–7%). Olivines have high MgO (Fo=78–85) and NiO content. Clinopyroxenes are high in MgO and CaO with the dominant ones having the formula of $En_{42-46}Wo_{41-50}Fs_{8-13}$. Plagioclases are dominantly andesine–labradorite (An=46–78%) and have normal zonation from bytownite in the core to andesine in the rim. Amphiboles are mainly magnesio and actinolitic hornblende, distinct from those in the Precambrian high-pressure granulites of the NCC. These gabbroic rocks are characterized by high MgO (9.0–11.04%) and SiO_2 (52.66–55.52%), and low Al_2O_3, FeOt and TiO_2, and could be classified as high-mg basaltic andesites. They are enriched in LILEs and LREEs, depleted in HFSEs and HREEs, and exhibit $(^{87}Sr/^{86}Sr)_i$=0.70492–0.70539, $\varepsilon_{Nd}(t)$=−12.47–15.07, $(^{206}Pb/^{204}Pb)_i$=16.63–17.10, Δ8/4=70.1–107.2 and Δ7/4=−2.1 to −9.4, i.e., an EMI-like isotopic signatures. Such geochemical features indicate that these early Cretaceous gabbroic rocks were originated from a refractory pyroxenitic veined-plus-peridotite source previously modified by an SiO_2-rich melt that may have been derived from Paleoproterozoic subducted crustal materials. Late Mesozoic lithospheric extension might have induced the melting of the metasomatised lithospheric mantle in response to the upwelling of the asthenosphere to generate these gabbroic rocks in the southern Taihang Mountains.

Keywords: SHRIMP zircon dating; Early Cretaceous gabbroic rocks; EM1-like lithospheric mantle; Taihang Mountains; Central North China Craton

* Corresponding author. Tel.: +86 20 85290527; fax: +86 20 85290708.
E-mail address: yjwang@gig.ac.cn (Y. Wang).

0024-4937/$ - see front matter © 2005 Elsevier B.V. All rights reserved.
doi:10.1016/j.lithos.2005.07.001

1. Introduction

The North China Craton (NCC) is one of the most ancient cratons in the East Asia with the age of crustal rocks up to 3.8 Ga (Liu et al., 1991). In general, the presence of Archean crustal rocks has been associated with the occurrence of a thick Archean lithospheric mantle (Boyd and Gurney, 1986). However, in the NCC, a Paleozoic thick "cratonic" lithospheric mantle revealed by presence of diamondiferous kimberlites and their entrained mantle xenoliths was dramatically thinned to a <100 km Cenozoic "oceanic" lithospheric mantle (Fan et al., 2000; Menzies and Xu, 1998; Griffin et al., 1992). The lithospheric nature change and its possible mechanism have attracted considerable attentions over the last two decades (Fan et al., 2000; Xu, 2001 and references therein). Recently, a series of studies has been undertaken on the late Mesozoic volcanics/mafic dikes from the margin of

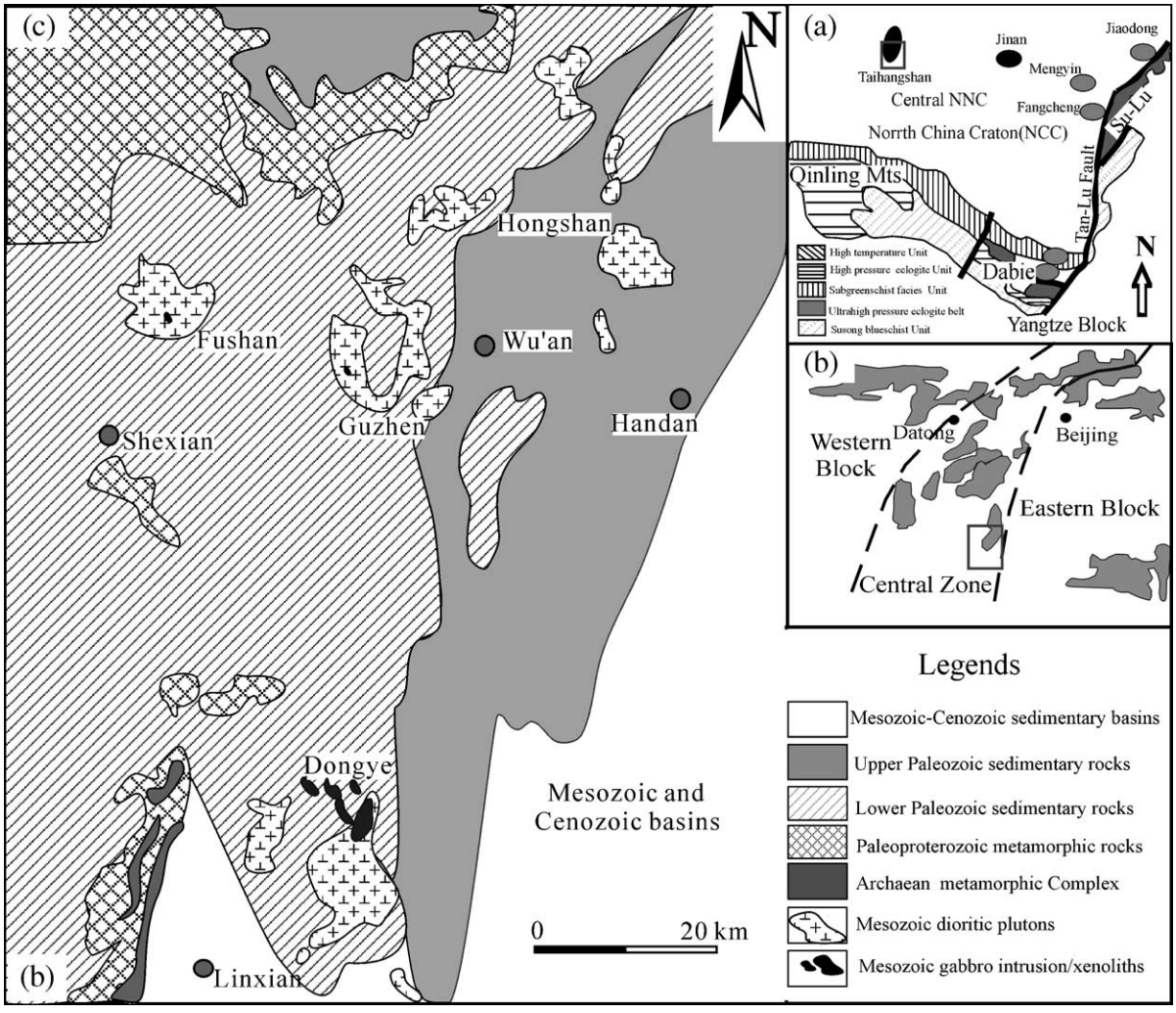

Fig. 1. (a) Subdivision of the NCC and their surroundings (modified after Jahn et al., 1999 and Wang et al., 2005); (b) three-fold tectonic subdivision of the North China Craton (NCC) (after Zhao et al., 2001a, 2005). The geographic locality of the southern Taihang Mountains is outlined in (a) and (b); (c) geological map of the southern Taihang Mountains showing the distribution of early Cretaceous gabbroic and dioritic-granitic intrusions (HBGMR, 1989).

the NCC (e.g., the Fangcheng basalts, Jiaodong mafic rocks, Fuxin high-mg andesites, and Dabie mafic-intermediate rocks, Fig. 1a) to better understand the nature of Mesozoic lithospheric mantle and thinning mechanism of the ancient lithosphere (Fan et al., 2001, 2004; Zhang et al., 2002, 2003; Qiu et al., 2002; Yang et al., 2004; Wang et al., 2005). These studies demonstrate that early Cretaceous volcanic rocks from the margin of the NCC may have been derived from an enriched lithospheric mantle, which were recently modified by the subducted crustal materials. More recently, limited studies on the northern Taihang Mesozoic lamprophyres and the Jinan gabbros from the central NCC (Fig. 1a) show that their sources have an affinity to an EMI-like mantle source (Chen and Zhai, 2003; Zhang et al., 2004; Guo et al., 2001; Chen et al., 2004). However, the geochemical investigations of the Mesozoic mafic rocks in the central NCC are still rare so far, and the spatial distribution of the EMI-like lithospheric mantle beneath the central NCC has long been debated (Zhang et al., 2004; Xu et al., 2004). The nature of the Mesozoic lithospheric mantle beneath the southern Taihang Mountains is still unknown.

Mesozoic plutonism is widely distributed in the central NCC. These plutonic rocks, such as gabbro, diorite, monzonite, syenite and granodiorite, are targeted to trace the nature of the lithospheric mantle beneath the region (Zhang et al., 2004; Chen and Zhai, 2003; Chen et al., 2004; Xu et al., 2004; Peng et al., 2004). However, Mesozoic gabbroic rocks, which have important implications on the mantle source, are less abundant. Additionally, except that there occurred Mesozoic high-mg volcanic rocks in Xinglonggou along a narrow belt in the northern margin of the NCC (Gao et al., 2004), Mesozoic high-mg rocks that are usually regarded as the product of young oceanic crust melting or the interaction between a subducted slab melt and mantle peridotite (McCarron and Smellie, 1998; Tsuchiya et al., 2005; Defant and Drummond, 1990) are rarely reported in the central NCC. In this paper, we present the mineralogical and geochemical data of high-mg gabbroic rocks from the southern Taihang Mountains, together with the results of the SHRIMP zircon U–Pb dating, to constrain the petrogenesis of these gabbroic rocks and further reveal the nature of the Mesozoic lithospheric mantle beneath the region.

2. Geological background

Description of the general geology of the NCC is available in literature (HBGMR, 1989; Liu et al., 1991; Zhao et al., 2000, 2001a; Wang et al., 2003, 2004 and reference therein). The NCC is composed of two Archean nuclei, named the Eastern and Western Blocks, separated by a Paleoproterozoic (~1850 Ma) orogenic belt referred to as the Central Zone or Trans-North China Orogen, of which the Taihangshan Mountains are located in the middle segment (Fig. 1b; Zhao et al., 2000, 2001a). The basement of the NCC is composed of amphibolite to granulite facies Archean grey tonalitic gneisses and greenstones and Paleoproterozoic khondalites and an overlying unmetamorphosed sedimentary cover from Mesoproterozoic onwards (Zhao et al., 1999, 2001b). It was generally considered that the Eastern and Western Blocks developed independently from the late Archean to early Paleoproterozoic and collided to form a coherent craton at ~1.85 Ga (Zhao et al., 1999, 2000, 2001a; Wang et al., 2003, 2004), and in the Mesozoic, the NCC encountered tectonothermal remobilization (Gilder et al., 1991; Davis et al., 2001; Zheng et al., 1996).

The southern Taihang Mountains is part of the Central Zone of the NCC (Fig. 1b) and represents a Paleoproterozoic subduction/collision boundary between the Eastern and Western blocks of the NCC (Zhao et al., 1999, 2001b; Wang et al., 2003, 2004). Mesozoic intrusions in the region (e.g., Fushan, Guzhen, Shexian, Jicun, Xi'anli and Dongye) are widespread (Fig. 1c), including gabbros, hornblende diorites, monzonites and syenites (HBGMR, 1989). The gabbros are of small volume and occur as laccoliths, knobs, or as xenoliths hosted in Mesozoic hornblende-dioritic intrusions (HBGMR, 1989; Tan and Lin, 1994; Sun and Hong, 1999). In this study, most of the samples were collected from the Dongye gabbroic laccoliths (~20 km^2 in the acreage) in Linxian County, Henan Province, with a few gabbroic samples (20HD8, 20HD70, 20HD78, 20HD79) from the Guzhen and Fushan dioritic intrusions (Fig. 1c). The gabbroic samples are gen-

erally fresh and are medium- to coarse-grained rocks. Their mineral compositions are plagioclase (40–50% in volume), amphibole (20–30%), clinopyroxene (10–15%), olivine (5–8%), biotite (5–7%) and feldspar (<5%). Accessory phases include zircon, apatite, magnetite, ilmenite and sphene. The plagioclase and clinopyroxene are coprecipitated and clinopyroxene contains plagioclase inclusions. Alkaline feldspar can be observed in several samples.

3. Analytical methods

Zircons were separated from sample 20HD41 using the conventional heavy liquid and magnetic techniques and purified by handpicking under a binocular microscope. The internal structure of zircons was examined using the cathodoluminescence (CL) image technique prior to U–Pb isotopic analyses. The U–Pb isotopic determination was undertaken on the polished mount using a sensitive high-resolution ion microprobe (SHRIMP II) at the Institute of Geology, the Chinese Academy of Geological Sciences (CAS). Spot size in the range of 20–30 μm was used for data collection, and before analyzing, each spot was rastered over 120 μm for 5 min to remove any common Pb on the surface. Detailed analytical procedures are similar to those described in Compston et al. (1984). The standard TEM zircons (age of 417 Ma) of RSES were used to determine the elemental discrimination that occurs during sputter ionization. Common Pb correction was made using the observed ^{204}Pb peak and the terrestrial Pb growth curve of Cumming and Richards (1975). Data processing was carried out using the SQUID 1.03 and Isoplot/Ex 2.49 programs of Ludwig (2001a, b). The analytical results are listed in Table 1.

Analyses of mineral compositions were carried out at the Institute of Geology and Geophysics (IGG), CAS using a Cameca SX50. Wavelength dispersive spectrometers were used with 15 kV accelerating voltage and 20 nA beam current. Representative mineral compositions are given in *Background Dataset*. Major oxide contents were analyzed at the Hubei Institute of Geology and Mineral Resource, the Chinese Ministry of Land and Resources by a wavelength X-ray fluorescence spectrometry with the relative standard derivations (RSD) of <5%. FeO content is solely analyzed by a wet chemical method. Trace element analyses were performed at the Institute of Geochemistry, CAS using an inductively coupled plasma mass spectrometry (Elan6000 ICP-MS). About 100 mg samples are digested with 1 ml of HF and 0.5 ml

Table 1
SHRIMP U–Pb data of zircons in the gabbro (20HD41) from the southern Taihang Mountains

Spot	U (ppm)	Th (ppm)	Th/U	^{206}Pb (ppm)	^{204}Pb/^{206}Pb	^{207}Pb/^{206}Pb	^{208}Pb/^{206}Pb	^{207}Pb/^{235}U	^{206}Pb/^{238}U	Discordant (%)	^{206}Pb/^{238}U age (Ma)
E1.1	137	149	1.12	2.36	0.0038	0.0779 ± 9	0.4232 ± 3	0.0608 ± 2	0.0201 ± 5	105	119.3 ± 6
E2.1	121	135	1.15	2.20	0.0032	0.0986 ± 10	0.4296 ± 16	0.0664 ± 2	0.0211 ± 5	59	127.1 ± 7
E3.1	146	157	1.11	2.51	0.0036	0.0947 ± 6	0.4829 ± 4	0.0567 ± 4	0.0200 ± 5	138	118.8 ± 6
E4.1	138	149	1.11	2.42	0.0030	0.0828 ± 4	0.4561 ± 4	0.0613 ± 2	0.0205 ± 5	126	123.3 ± 6
E5.1	259	312	1.25	4.90	0.0029	0.0740 ± 6	0.4746 ± 2	0.0566 ± 1	0.0221 ± 5	111	133.1 ± 7
E6.1	113	118	1.07	2.00	0.0043	0.0936 ± 5	0.4645 ± 3	0.0541 ± 2	0.0206 ± 5	110	121.0 ± 7
E7.1	225	231	1.06	3.77	0.0009	0.0639 ± 4	0.3712 ± 3	0.0574 ± 2	0.0195 ± 5	49	122.6 ± 6
E8.1	141	138	1.01	2.45	0.0017	0.0703 ± 5	0.4014 ± 3	0.0585 ± 2	0.0202 ± 5	293	125.0 ± 6
E9.1	113	124	1.13	2.03	0.0025	0.0860 ± 4	0.4552 ± 3	0.0648 ± 2	0.0208 ± 5	1	126.4 ± 6
E10.1	250	323	1.34	4.31	0.0011	0.0725 ± 4	0.4738 ± 2	0.0590 ± 2	0.0201 ± 5	72	125.5 ± 7
E11.1	217	342	1.62	3.55	0.0025	0.0714 ± 4	0.6170 ± 2	0.0605 ± 2	0.0190 ± 5	115	115.9 ± 7
E12.1	249	290	1.20	4.48	0.0015	0.0705 ± 5	0.4058 ± 7	0.0620 ± 1	0.0209 ± 5	5	129.9 ± 7
E13.1	121	111	0.95	2.24	0.0020	0.0795 ± 6	0.4244 ± 4	0.0416 ± 2	0.0216 ± 5	37	132.5 ± 7
E14.1	211	292	1.43	3.95	0.0037	0.0862 ± 3	0.5543 ± 3	0.0652 ± 1	0.0218 ± 5	112	129.5 ± 7

The data were calculated using the ^{204}Pb correction method. The common Pb was estimated from ^{204}Pb counts, assuming an isotopic composition of Broken Hill lead related to surface contamination (Nelson, 1997).

Table 2
Major and trace element abundances of early Cretaceous gabbroic rocks from the southern Taihang Mountains

Samples	20HD 47	20HD 40	20HD 42	20HD 46	20HD 45	20HD 50	20HD 41	20HD 43	20HD 51	20HD 79	20HD 78	20HD 8	20HD 70	DG1	DG2	DG3	DG4
SiO_2	53.37	53.49	53.70	53.77	53.82	53.89	53.92	54.19	54.70	52.06	52.32	53.28	54.40	52.92	52.25	52.98	52.48
TiO_2	0.57	0.59	0.59	0.60	0.58	0.59	0.57	0.57	0.59	0.61	0.60	0.61	0.59	0.56	0.61	0.58	0.59
Al_2O_3	13.37	13.48	13.22	13.30	13.42	13.68	13.36	13.42	13.59	12.30	12.58	13.32	13.57	13.31	12.93	13.27	13.13
Fe_2O_3	3.00	2.89	3.00	3.06	3.00	2.64	2.72	2.85	2.39	4.00	3.53	4.16	3.01	4.42	4.60	4.59	4.34
FeO	5.40	5.47	5.33	5.23	5.27	5.30	5.33	5.10	5.33	5.45	5.50	4.54	5.06	3.79	4.21	3.87	3.96
MgO	9.09	9.02	8.90	8.86	8.83	9.44	8.94	8.87	9.01	10.69	10.38	9.81	9.01	9.78	10.81	9.80	10.71
CaO	7.79	7.74	7.98	7.69	7.80	7.40	7.57	7.56	7.03	9.10	9.20	8.13	7.30	7.90	7.92	7.86	8.13
Na_2O	2.96	2.97	3.07	3.00	3.04	3.12	3.08	2.98	3.22	3.55	3.55	3.74	3.84	2.37	2.53	2.49	2.51
K_2O	1.96	1.99	1.90	1.98	2.03	1.94	1.98	2.16	2.27	0.77	0.97	1.06	1.54	1.89	1.86	1.83	1.65
MnO	0.16	0.16	0.15	0.15	0.15	0.15	0.15	0.14	0.14	0.16	0.15	0.14	0.16	0.12	0.12	0.12	0.11
P_2O_5	0.26	0.26	0.26	0.26	0.26	0.26	0.25	0.26	0.27	0.18	0.20	0.18	0.30	0.24	0.22	0.24	0.23
LOI	1.79	1.63	1.60	1.82	1.52	1.27	1.84	1.19	1.08	1.11	1.09	1.07	1.12	2.19	1.96	2.28	2.15
Total	99.72	99.69	99.70	99.72	99.72	99.68	99.71	99.29	99.60	99.97	100.1	99.97	99.85	99.49	99.92	99.91	99.99
mg	68	68	68	68	68	70	68	69	70	69	70	67	68	70	69	71	.70
Sc	22	21	21	21	22	20	20	19	18	26	28	40	21	23	23	22	23
V	165	176	172	177	174	162	168	159	145	308	328	278	175	201	276	193	253
Cr	455	457	468	457	466	505	478	456	468	605	565	520	542	500	487	512	508
Co	39	40	39	40	40	40	40	38	38	57	54	55	39	48	53	47	50
Ni	198	192	189	201	194	295	201	200	279	266	170	258	237	230	224	198	237
Rb	41	41	37	41	41	41	40	40	44	5.7	15	7.9	40	39	36	33	30
Sr	684	687	697	695	698	749	697	694	709	444	580	630	758	667	587	635	661
Zr	66.4	64.7	74.6	77.1	73.6	70.3	64.2	61.3	74.9	75.3	67.5	80.0	72.2	71	72	79	65
Nb	3.34	3.84	4.57	3.75	4.01	4.12	3.17	3.01	4.31	4.01	3.86	3.25	3.60	3.20	2.90	3.00	2.30
Ba	634	611	631	720	626	728	691	899	687	586	409	392	639	513	470	496	482
Y	14.28	18.45	16.59	14.81	15.62	15.48	13.81	12.10	15.15	16.41	15.39	17.25	14.79	16.87	16.73	16.07	15.56
La	19.20	19.50	20.43	20.19	20.63	22.37	19.90	19.45	22.65	16.16	16.94	14.42	20.10	18.58	18.98	17.93	17.48
Ce	39.42	40.01	43.06	41.70	42.23	46.28	41.04	38.64	46.21	34.39	37.47	30.49	40.94	42.93	35.1	34.41	34.46
Pr	4.51	4.59	5.15	4.79	5.07	5.29	4.78	4.52	5.24	4.29	4.58	4.18	4.76	3.66	4.12	3.98	3.83
Nd	19.04	19.73	22.30	19.94	20.39	22.36	19.84	17.76	21.54	20.14	19.96	19.77	20.98	14.58	17.42	15.10	13.56
Sm	3.90	4.26	4.38	4.44	4.08	4.34	3.90	3.67	4.25	4.51	4.26	5.34	4.02	3.74	3.61	3.83	3.92
Eu	1.33	1.40	1.46	1.47	1.43	1.46	1.27	1.23	1.42	1.56	1.38	1.45	1.39	1.19	1.22	1.26	1.32
Gd	3.09	3.04	3.57	3.29	3.60	3.42	2.98	2.69	3.13	3.22	3.32	4.01	3.10	3.34	3.11	3.22	2.99
Tb	0.47	0.51	0.55	0.54	0.55	0.52	0.49	0.43	0.48	0.60	0.51	0.68	0.50	0.45	0.46	0.45	0.42
Dy	2.62	2.78	3.15	2.97	3.19	3.11	2.64	2.37	2.87	3.19	3.01	3.64	2.71	2.34	2.63	2.67	2.33
Ho	0.54	0.55	0.65	0.58	0.56	0.59	0.47	0.48	0.50	0.56	0.58	0.70	0.51	0.45	0.55	0.50	0.56
Er	1.44	1.54	1.74	1.54	1.61	1.61	1.52	1.43	1.58	1.67	1.63	1.91	1.55	1.1	1.29	1.74	1.48
Tm	0.22	0.21	0.28	0.21	0.27	0.20	0.22	0.19	0.23	0.25	0.25	0.25	0.22	0.16	0.20	0.21	0.19
Yb	1.39	1.44	1.59	1.57	1.49	1.44	1.39	1.23	1.41	1.63	1.51	1.53	1.48	1.03	1.42	1.11	1.34
Lu	0.23	0.21	0.25	0.20	0.22	0.22	0.18	0.17	0.19	0.20	0.20	0.19	0.21	0.17	0.23	0.19	0.22
Hf	1.75	1.70	1.96	2.03	1.94	1.85	1.69	1.61	1.97	2.27	2.29	2.95	2.14	1.80	1.80	2.00	1.50
Ta	0.19	0.20	0.25	0.20	0.23	0.22	0.16	0.18	0.25	0.21	0.21	0.18	0.17	0.21	0.20	0.18	0.21
Pb	5.87	7.33	5.52	5.80	5.89	8.96	4.97	5.38	7.72	3.76	4.22	3.98	7.11	7.10	5.60	7.80	8.04
Th	2.20	2.25	2.36	2.27	2.49	2.61	1.97	2.41	2.70	1.94	1.97	3.56	2.19	2.80	2.60	2.30	1.50
U	0.72	0.71	0.77	0.75	0.80	0.76	0.67	0.67	0.73	0.51	0.53	0.60	0.63	0.80	0.60	0.50	0.50
$(Nb/La)_{PM}$	0.17	0.19	0.22	0.18	0.19	0.18	0.15	0.15	0.18	0.25	0.22	0.22	0.17	0.17	0.15	0.16	0.13
(La/Yb)cn	9.76	9.62	9.08	9.14	9.78	10.97	10.12	11.21	11.41	6.60	7.96	6.69	9.63	12.78	9.47	11.44	9.24

HNO_3 in screw top PTFE-lined stainless steel bombs at 190 °C for 12 h. Insoluble residues are dissolved using 8 ml of 40% HNO_3 (v/v) heated to 110 °C for 3 h. Rh and In are used as internal standard for correcting instrumental signal drift, which was usually <10% over a period of 6 h. Detailed sample preparation and analytical procedures follow Qi et al. (2000). The analytical precision is better than 5% for elements >10 ppm, less than 8% for those <10 ppm, and about 10% for transition metals. The analytical results of the samples are listed in Table 2.

Sample powders for Sr and Nd isotopic analyses were spiked with mixed isotope tracers, dissolves in Teflon capsules with HF+HNO_3 acids, and separated by a conventional cation exchange technique and run on single W and Ta–Re double filaments, respectively. The total procedure blanks are in the range of 200–500 pg for Sr and less than 50 pg for Nd. Isotopic compositions were measured on the VG-354 mass spectrometer at the IGG, CAS. The mass fractionation corrections for Sr and Nd isotopic ratios were based on $^{86}Sr/^{88}Sr=0.1194$ and $^{146}Nd/^{144}Nd=0.7219$, respectively. Measured $^{87}Sr/^{86}Sr$ ratio of (NIST) SRM 987 standard and $^{143}Nd/^{144}Nd$ ratio of the La Jolla standard are 0.710265 ± 12 (2σ, external precision) and 0.511862 ± 10 (2σ), respectively. During the course of this study within-run errors of precision are estimated to be better than 0.000015 for $^{86}Sr/^{88}Sr$ and $^{146}Nd/^{144}Nd$ in the 95% confidence level. $^{143}Nd/^{144}Nd$ and $^{147}Sm/^{144}Nd$ ratios of CHUR at the present time used for calculating ε_{Nd} value are 0.512638 and 0.1967, respectively. For Pb isotopic determination, ~200 mg powder was weighted into the Teflon cup, spiked and dissolved in concentrated HF at 180 °C for 3 days. Pb was separated and purified by conventional cation-exchange techniques (200–400 mesh AG1-X8 anion exchange resin) with diluted HBr as eluant. Detailed descriptions of the analytical techniques can be found in Zhang et al. (2002). Pb isotopic ratios were measured using the VG-354 mass spectrometer at the IGG, CAS. Repeated analyses of SRM 981 yielded $^{206}Pb/^{204}Pb=16.942\pm4$ (2σ), $^{207}Pb/^{204}Pb=15.498\pm4$ (2σ) and $^{208}Pb/^{204}Pb=36.728\pm9$ (2σ). External precisions are estimated to be less than 0.005, 0.005 and 0.0015. The Sr, Nd and Pb isotopic analytical results are presented in Table 3.

Table 3
Sr, Nd and Pb isotopic compositions of early Cretaceous gabbroic rocks from the southern Taihang Mountains

Sample	Sm	Nd	Rb	Sr	$^{147}Sm/^{144}Nd$	$^{143}Nd/^{144}Nd\pm2\sigma$	$^{87}Rb/^{86}Sr$	$^{87}Sr/^{86}Sr\pm2\sigma$	$(^{87}Sr/^{86}Sr)_i$	$\varepsilon_{Nd}(t)$	$^{238}U/^{204}Pb$	$^{232}Th/^{204}Pb$	$^{206}Pb/^{204}Pb$	$^{207}Pb/^{204}Pb$	$^{208}Pb/^{204}Pb$	$(^{206}Pb/^{204}Pb)_i$	$(^{207}Pb/^{204}Pb)_i$	$(^{208}Pb/^{204}Pb)_i$	Δ7/4	Δ8/4
20HD47	3.90	19.04	41.0	683.7	0.124	0.511929±7	0.174	0.705245±15	0.704936	−12.67	7.438	23.430	16.778	15.265	36.936	16.632	15.258	36.791	−3.6	105.5
20HD42	4.38	22.30	37.2	696.6	0.119	0.511917±11	0.155	0.705486±20	0.705211	−12.83	8.412	26.779	16.996	15.273	36.943	16.831	15.265	36.777	−5.1	80.1
20HD46	4.44	19.94	40.9	694.5	0.135	0.511948±9	0.171	0.705297±18	0.704994	−12.47	7.806	24.577	16.984	15.286	36.953	16.831	15.279	36.801	−3.7	82.5
20HD45	4.08	20.38	41.1	697.5	0.121	0.511929±10	0.171	0.705343±21	0.705040	−12.63	8.243	26.433	16.963	15.276	36.943	16.802	15.268	36.779	−4.4	83.9
20HD41	3.90	19.83	39.8	697.5	0.119	0.511918±6	0.166	0.705557±16	0.705263	−12.81	8.114	24.786	16.991	15.292	36.973	16.832	15.284	36.819	−2.1	84.2
20HD43	3.67	17.76	39.8	694.0	0.129	0.511872±12	0.166	0.705437±18	0.705142	−13.80	7.503	28.129	16.973	15.292	37.026	16.826	15.285	36.852	−3.0	88.2
20HD51	4.25	21.54	43.8	709.1	0.119	0.511810±9	0.179	0.705426±17	0.705108	−14.92	5.755	21.906	16.762	15.249	36.887	16.649	15.244	36.751	−5.2	99.5
20HD78	4.26	19.96	15.3	580.4	0.129	0.511938±8	0.076	0.705532±22	0.705387	−12.58										
20HD8	5.34	19.77	7.93	630.1	0.164	0.511917±11	0.073	0.705142±19	0.705012	−13.54										
DG1	3.74	18.18	39.1	667.1	0.122	0.511906±10	0.158	0.705447±17	0.705166	−13.09	6.918	25.020	17.236	15.287	37.529	17.101	15.280	37.374	−9.4	107.2
DG2	4.28	21.40	36.2	587.0	0.121	0.511804±9	0.178	0.705527±15	0.705211	−15.07	6.512	29.158	17.022	15.273	36.934	16.894	15.266	36.753	−5.6	70.1
DG3	3.83	17.51	33.3	635.2	0.119	0.511883±9	0.141	0.705169±20	0.704919	−13.50	3.924	18.651	17.154	15.283	37.379	17.077	15.279	37.264	−7.3	99.1
DG4	10.74	53.02	30.1	661.3	0.120	0.511900±10	0.126	0.705191±13	0.704968	−13.18	3.817	11.831	17.083	15.295	37.261	17.008	15.291	37.188	−4.4	99.8

Chondrite uniform reservoir values, $^{147}Sm/^{144}Nd=0.1967$, $^{143}Nd/^{144}Nd=0.512638$, are used for the calculation. $\varepsilon_{Nd}(t)$ is calculated by assuming 125 Ma. Sm, Nd, Rb, and Sr: ppm. $\lambda_{U238}=1.55125*10^{-10}$/year, $\lambda_{U235}=9.848*10^{-10}$/year, $\lambda_{Th232}=4.9475*10^{-11}$/year (Steiger and Jäger, 1977). Initial Pb isotopic ratios were calculated using the measured whole-rock Pb isotopic compositions, whole-rock U, Th and Pb contents by assuming 125 Ma. $\Delta7/4=((^{207}Pb/^{204}Pb)_i-(^{207}Pb/^{204}Pb)_{NHRL})*100$; $\Delta8/4=((^{208}Pb/^{204}Pb)_i-(^{208}Pb/^{204}Pb)_{NHRL})*100$; $(^{207}Pb/^{204}Pb)_{NHRL}=0.1084*(^{206}Pb/^{204}Pb)_i+13.491$, $(^{208}Pb/^{204}Pb)_{NHRL}=1.209*(^{206}Pb/^{204}Pb)_i+15.627$ (Hart, 1984).

4. Results

4.1. Zircon U–Pb geochronology

Zircons from a medium-grained gabbro (20HD41), the Dongye intrusion, exhibit similar morphology, mostly euhedral and up to 100 μm in length with ~2:1 of length/width ratio. Most crystals are transparent and light brown in color, and have oscillatory zoning (inset in Fig. 2a). Fourteen analyses on 14 grains give a relatively wide range in U (113–259 ppm) and Th (111–342 ppm) concentration. Th/U ratios of these zircons are rather constant (~1.10) except two grains in which Th/U ratios are greater than 1.40 (Fig. 2a). These analyses form a single and tight cluster on the concordia plot (Fig. 2b), and yield a weighted mean $^{206}Pb/^{238}U$ age of 125.2 ± 4.5 Ma (n = 14) with an MSWD = 0.28. This age is interpreted as the crystallization age of the Dongye gabbroic intrusion, similar to those of the Fushan and Dongye dioritic plutons (125.7 ± 1.1Ma and 125.9 ± 0.9 Ma, respectively) in the region (Peng et al., 2004).

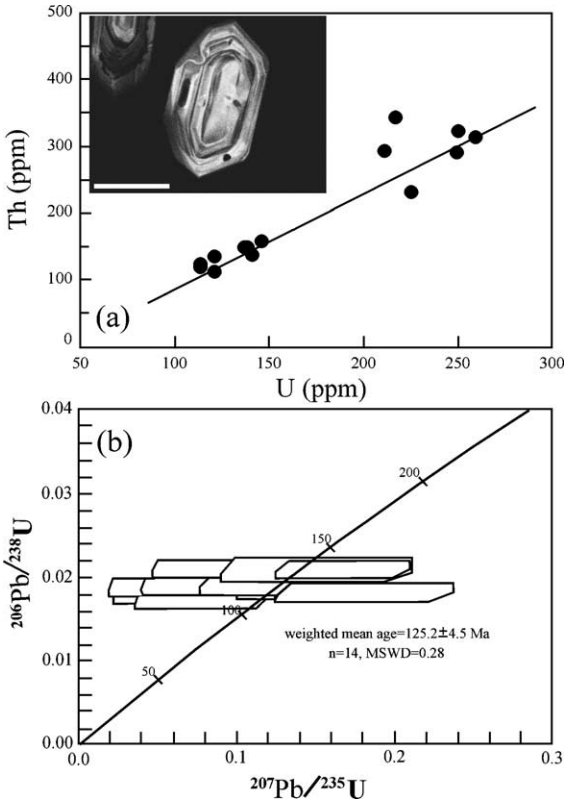

Fig. 2. Zircon Th–U plot (a) and SHRIMP zircon U–Pb concordia diagram (b) for the gabbroic sample 20HD41. Inset in (a) shows the CL image of representative zircon. *Scale bar* = 100 μm.

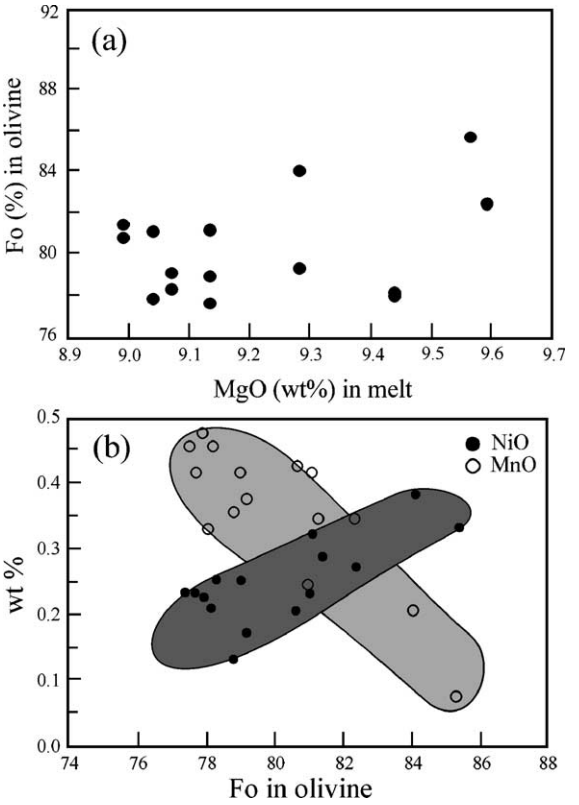

Fig. 3. (a) The MgO content of the whole rocks against Fo in the olivines, and (b) MnO and NiO contents of olivines from the studied samples.

4.2. Mineralogy

Olivines have high NiO (0.13–0.38%) content and show a wide compositional variation, such as forsterite (Fo) ranging from 78 to 85 mol% irrespective of MgO content in melt (Fig. 3a). The NiO increases while MnO decreases with the increasing of Fo contents (Fig. 3b). Clinopyroxenes have MgO = 14.4–15.9%, CaO = 20.0–23.7% and total FeO = 4.8–8.1%, and mg numbers [mg = 100 * Mg^{2+}/($Fe^{2+}Mg^{2+}$)] range between 77 and 84, and thus the clinopyroxenes are diopside to salites in composition (Deer et al., 1978).

Amphiboles are pale green, subhedral to euhedral and have corona textures. Amphiboles are high in

MgO (14.8–16.3%), CaO (10.9–12.9%) and low in TiO_2 (0.6–1.2%), with mg numbers in a range from 76 to 88. According to classification of Leake et al. (1978), they are calcic hornblende with Ca > 1.71 and Na_B = 0.03–0.29. In a plot of Si^{VI} vs. A site and $Mg/(Mg+Fe^{2+})$ diagrams (Fig. 4), the amphiboles are mainly magnesio and actinolitic hornblende, and Na^A+K^A decreases but $Mg/(Mg+Fe^{2+})$ increases with increase in Si^{IV}. These features are distinct from those of amphiboles from the Precambrian high-pressure mafic granulites of the NCC, which are characterized by low mg (<60), and Si^{IV}-poor (<6.6) and Fe-rich (Zhao et al., 2001b).

Plagioclases are high in Al_2O_3 (22.4–27.7%) and Na_2O (4.5–8.7%), and low in CaO (3.8–11.9%) and K_2O (<0.7%) with An of 40–78 mol%, Ab of 18–59 mol% and Or of 1–4 mol%, and commonly show

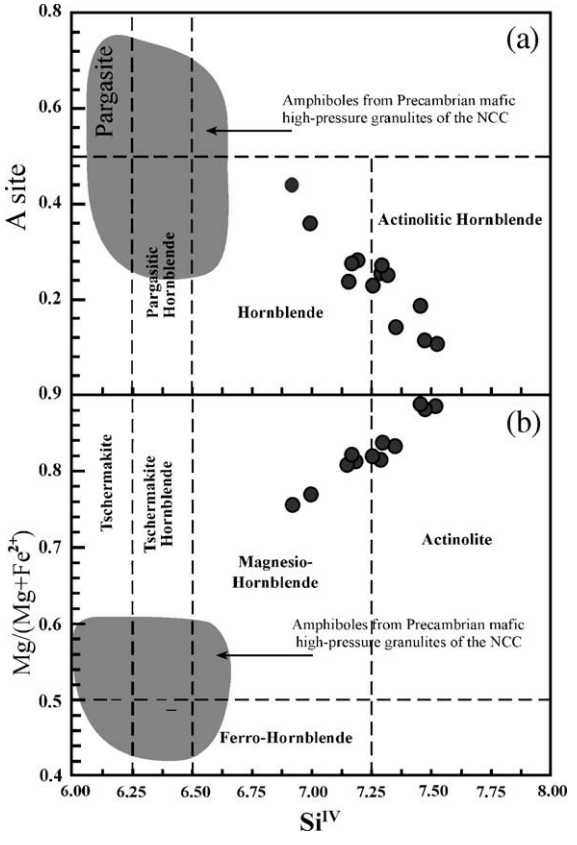

Fig. 4. Si^{IV} vs. (a) A site and (b) $Mg/Mg+Fe^{2+}$ plots for amphiboles (Leake, 1978). The compositions of amphiboles from the Precambrian high-pressure granulites of the NCC are from Zhao et al. (2001b).

normal zonation with calcic/bytowic plagioclase mantle (An = 60–78) and sodic/calcic plagioclase rim (An = 40–56). Biotites are mostly annite in composition showing Al^T = 2.4–2.7, $Fe^{2+}/(Fe^{2+}Mg^{2+})$ = 0.41–0.45] and TiO_2 = 4.2–5.1%. A site in biotite is mainly presented in the tetrahedral site.

4.3. Geochemical characteristics

The gabbroic rocks have SiO_2 of 52.66–55.52% (volatile-free), and total alkalis (Na_2O+K_2O) of 4.25–5.57% with K_2O/Na_2O of 0.22–0.80 (Table 2), and belong to the sub-alkaline basaltic andesites (Fig. 5a). They are high in MgO (9.00–11.04%) and low in Al_2O_3 (12.44–13.90%), TiO_2 (0.58–0.62%), total FeO (FeOt = 7.84–9.56%) and P_2O_5 (0.18–0.30%) with mg numbers of 67–71, Ni of 170–295 ppm, and Cr of 455–605 ppm. Thus, they can be classified as high-mg basaltic andesites according to definition of Crawford et al. (1989). In Fig. 5, these samples display coherent variation trends. MgO, CaO, FeOt, Cr and Ni negatively correlate with SiO_2, whereas Al_2O_3, K_2O+Na_2O and P_2O_5 positively correlate with SiO_2. The TiO_2 content is relatively constant with the increase of SiO_2 content.

The light rare-earth elements (LREE) are highly fractionated in these gabbroic rocks ($(La/Yb)_{cn}$ = 6.60–12.78), relative to heavy rare-earth elements (HREEs) (Fig. 6a). On the spidergram (Fig. 6b), these rocks also show pronounced enrichment in large-ion lithophile elements (LILEs) and strong depletion in high-field strength elements (HFSEs), similar to those of island arc-related volcanic rocks. The subparallel "spiky" patterns with Ba and Sr peaks and deep Nb–Ta [$(Nb/La)_{PM}$ = 0.13–0.22] trough are observed. Negative Zr–Hf [$(Hf/Sm)_{PM}$ = 0.55–0.79] and P–Ti anomalies are also apparent. Other striking features of these gabbroic rocks include low Yb (1.03–1.63 ppm) and Y (12.10–17.25 ppm), and high Sr (444–758 ppm) and Sr/Y (35.4–57.4) (Table 2), similar to adakites from island arcs and Archean TTG rocks. In comparison with the contemporaneous Jinan gabbros in the central NCC, these gabbroic rocks are more enriched in incompatible elements (Fig. 6).

The initial Sr isotopic ratios range from 0.704919 to 0.705387, and $\varepsilon_{Nd}(t)$ values vary from −12.47 to

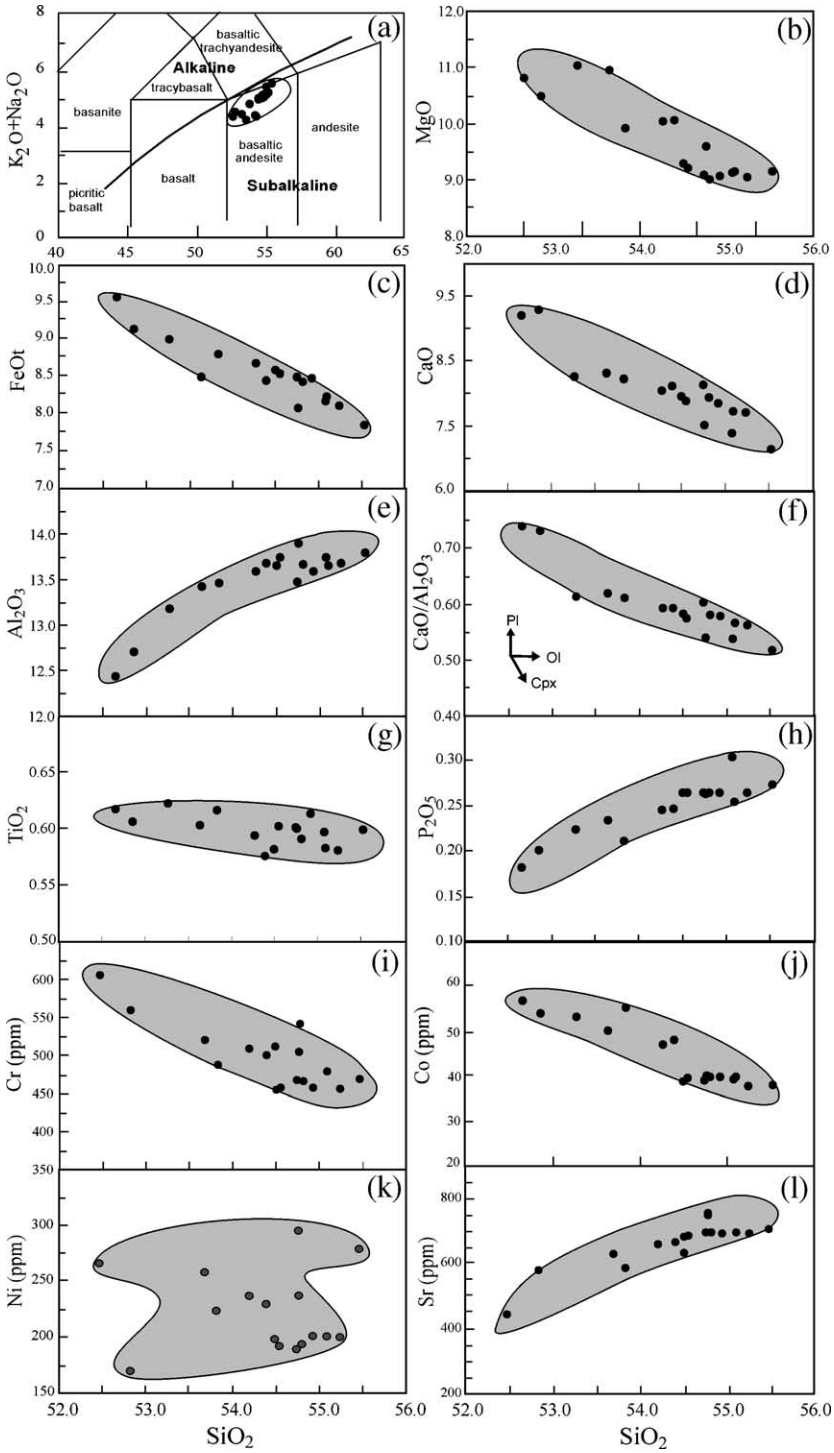

Fig. 5. SiO_2 vs. (a) K_2O+Na_2O, (b) MgO, (c) FeOt, (d) CaO, (e) Al_2O_3, (f) CaO/Al_2O_3, (g) TiO_2, (h) P_2O_5, (i) Cr, (j) Ni, (k) Co and (l) Sr for the gabbroic rocks of the southern Taihang Mountains.

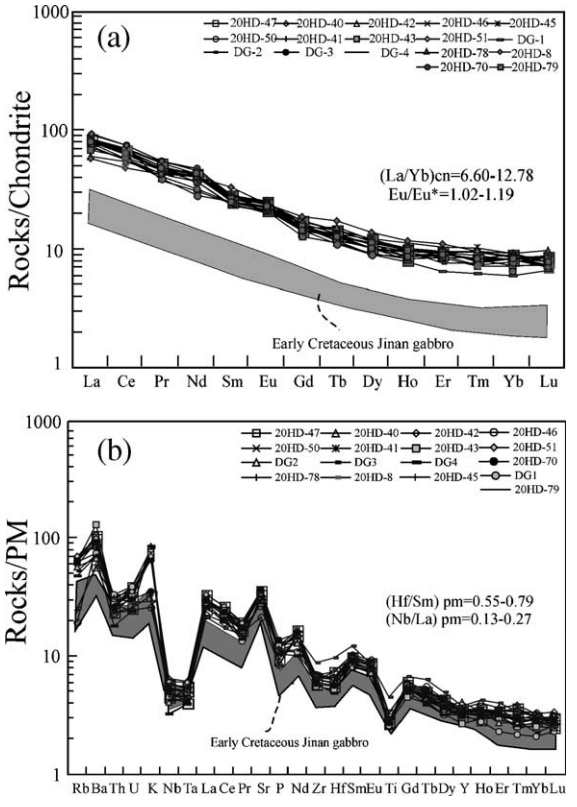

Fig. 6. (a) Chondrite normalized REE and (b) primitive mantle-normalized spidergram for the gabbroic rocks of the southern Taihang Mountains. Chondrite- and primitive mantle-normalize values are from Taylor and McLennan (1985) and Sun and McDonough (1989), respectively. The Jinan gabbros are from authors' unpublished data.

−15.07 (Table 3). Thus, the Sr–Nd isotopic compositions exhibit an affinity to EMI-like source (Fig. 7). These gabbroic rocks also have a low U/Pb ratio, prominent positive Δ8/4 (70.1–107.2) and slightly negative Δ7/4 (−2.1 to −9.4) values with $(^{206}Pb/^{204}Pb)_i$=16.63–17.10, $(^{207}Pb/^{204}Pb)_i$=15.24–15.29, and $(^{208}Pb/^{204}Pb)_i$=36.75–37.37 (Table 3). In a plot of $(^{206}Pb/^{204}Pb)_i$ vs. $(^{208}Pb/^{204}Pb)_i$ (Fig. 8a), they fall above the North Hemisphere Reference Line (NHRL). However, in a $(^{206}Pb/^{204}Pb)_i$ vs. $(^{207}Pb/^{204}Pb)_i$ plot (Fig. 8b), these samples form a well-defined linear array and fall below the NHRL (Hart, 1984). The Sr–Nd–Pb isotopic compositions for these rocks are similar to those of the contemporaneous gabbroic-dioritic rocks from the northern Taihang Mountains and the Jinan gabbros (Zhang et al., 2004), but they are different from those of early Cretaceous basic–intermediate rocks from the Dabie Orogen, Jiaodong and Fangcheng areas (Figs. 7 and 8; Jahn et al., 1999; Fan et al., 2001, 2004; Wang et al., 2005; Zhang et al., 2002, 2004).

5. Discussions

5.1. Fractional crystallization and crustal contamination

According to the amphibole geobarometer of Schmidt (1992), amphiboles in these gabbroic rocks are crystallized at ~1.4 ± 1.2 kbar, corresponding to a depth of ~2–8 km under the static pressure condition. Under such a high-level emplacement condition, the gabbroic magma may have experienced crystal fractionation from parental magma and crustal contamination during ascent.

The pattern of decreasing MgO and FeOt contents with increasing SiO_2 (Fig. 5b–c) supports fractionation of olivine. The correlation between SiO_2 and CaO, Al_2O_3 and CaO/Al_2O_3 (Fig. 5c–f) suggests the presence of clinopyroxene fractionation (Fig. 3d–f). The decrease of Cr, V and Co concentrations with magma evolution also reflects the importance of olivine and clinopyroxene fractionation (Fig. 5i–j). The irregular variation of Ni with the increase of SiO_2 (Fig. 5k), inconsistent with the normal trend of olivine fractionation, may be related to inhomogeneous distribution of olivine with variable NiO concentrations in the samples. Fractionation of apatite and Fe–Ti oxides may have not played an important role as suggested by relatively constant TiO_2 and the increase of P_2O_5 contents with the increase of SiO_2 (Fig. 5g–h). The depletions in P and Ti (Fig. 6b) may reflect the characteristics of the source rocks rather than the result of apatite and Ti–Fe-oxides fractionation. Since Sr is compatible in plagioclase, the increase of Sr content with the increase of SiO_2 (Fig. 5l) and the lack of negative Eu anomalies argue against a significant fractionation of plagioclase. The compositional characteristics of the gabbroic rocks, therefore, are consistent with olivine and clinopyroxene fractionation during magma evolution. However, such a fractionation alone fails to explain high MgO, mg number and Cr contents, and "crustal-like" isotopic systema-

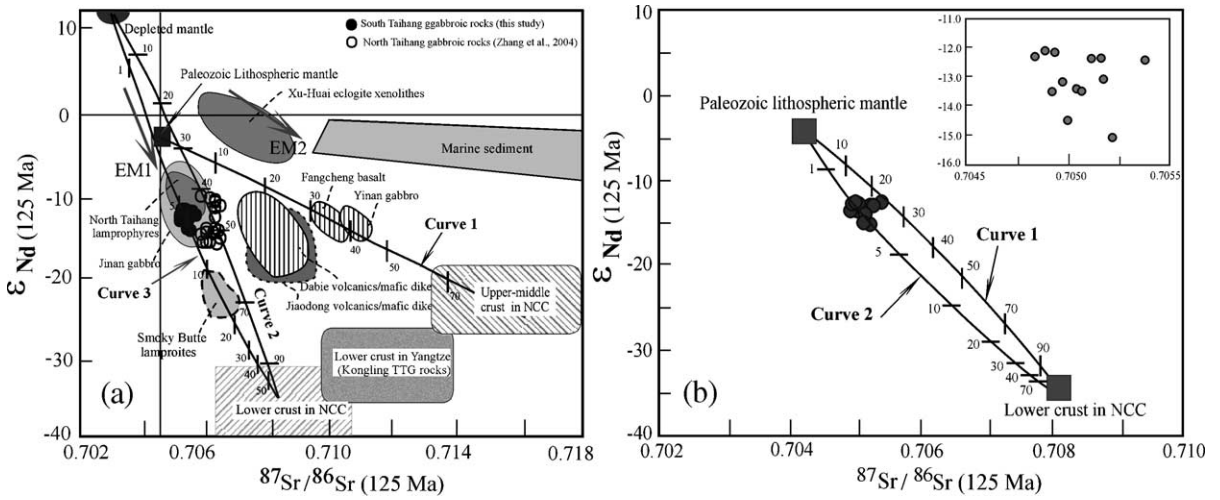

Fig. 7. Initial $^{87}Sr/^{86}Sr(t)$ vs. $\varepsilon_{Nd}(t)$ (t=125 Ma) diagram for the gabbroic rocks from the southern Taihang Mountains. Isotopic data of early Cretaceous northern Taihangshan lamprophyres (Chen and Zhai, 2003), Jinan gabbros (Guo et al., 2001; Zhang et al., 2004), Dabie volcanic/mafic dikes (Fan et al., 2004; Wang et al., 2005), Fangcheng basalts (Zhang et al., 2002), Yinan gabbros (Xu et al., 2004), Jiaodong volcanics/mafic dikes (Fan et al., 2001; Yang et al., 2004) are given for comparison. The field for the Kongling TTG rocks and Xu-Huai eclogite xenoliths are after Gao et al. (1998, 1999, 2004). Lower crust and upper-middle crust of the NCC are from Jahn et al. (1999) and Fan et al. (2001), respectively. Data of depleted mantle and marine sediment are after Zindler and Hart (1986) and McLennan et al. (1990). The numbers indicate the percentages of participation of crust. The calculated parameters of Sr (ppm), Nd (ppm), $^{87}Sr/^{86}Sr(t)$, and $\varepsilon_{Nd}(t)$ are 20, 1.0, 0.7028, +12 for depleted mantle (Sun and McDonough, 1989; Zindler and Hart, 1986); 20, 1.5, 0.7045, −5 for the Paleozoic lithospheric mantle in the NCC (represented by kimberlite-borne xenoliths; Zheng and Lu, 1997; Xu et al., 2004); 290, 21, 0.7080, −35 for the lower crust of the NCC (Jahn and Zhang, 1984; Chen and Zhai, 2003; Zhang et al., 1994), and 250, 26, 0.7160, −26 for the upper-middle crust of the NCC (Jahn and Zhang, 1984; Fan et al., 2001; Zhang et al., 1994), respectively. Sr and Nd contents for the derived melt from the mantle are 15 and 150 ppm (Xu et al., 2004). Curve 1 in (a) and curve 1 in (b) note the trends of crustal contamination between the Paleozoic lithospheric mantle-derived magma and the NCC upper-middle crust, the NCC lower crust, respectively. Curve 2 in (a) notes trend of crustal contamination between the depleted mantle-derived magma and the NCC lower crust. Curve 3 in (a) and Curve 2 in (b) note the trends of source mixing between the depleted mantle, and Paleozoic lithospheric mantle and the NCC lower crust, respectively.

tics for these rocks (Tables 2 and 3 and Figs. 5–8). Thus, the involvement of crustal components, either in source regions or crustal assimilation en route, is a likely alternative.

Upper crustal assimilation en route can be ruled out, on the basis of the high MgO (>9.0%), mg number (67–71), Cr (>450 ppm) and Sr (>600 ppm) and Ba (>400 ppm) contents of these gabbroic rocks (Table 2, Figs. 5l and 6b), which are much higher than the upper crust of the NCC (Zhang et al., 1994) and the average continental crust values (Rudnick and Fountain, 1995). This conclusion is also supported by the fact that all samples are plotted far away from the mixing trend between any kind of mantle-derived magma and upper-middle crust of the NCC (e.g., curve 1 in Fig. 7a). The lower crustal contamination may have played an important role, as data point toward the field for the lower crust of the NCC (Figs. 7 and 8). However, simple mixing calculations show that the assimilation of >20% lower crust of the NCC into mantle-derived magma is required to match with the observed Sr–Nd isotopic compositions of these gabbroic rocks (curve 2 in Fig. 7a and curve 1 in Fig. 7b). The involvement of such high proportional crustal materials cannot be reconciled with the mafic composition of these gabbroic rocks. Additionally, these gabbroic rocks have much higher abundances of the LILEs and LREE, and lower (Nb/La)n ratio (0.13–0.28) than those of the lower crust of the NCC (Gao et al., 1998; Zhang et al., 1994) and the average crust (Rudnick and Fountain, 1995; Taylor and McLennan, 1985). The lack of crustal inheritance in the zircon U–Pb systematics also argues against the significant crustal contamination.

More complex processes involving coupled assimilation and fractionation and crystallization (AFC,

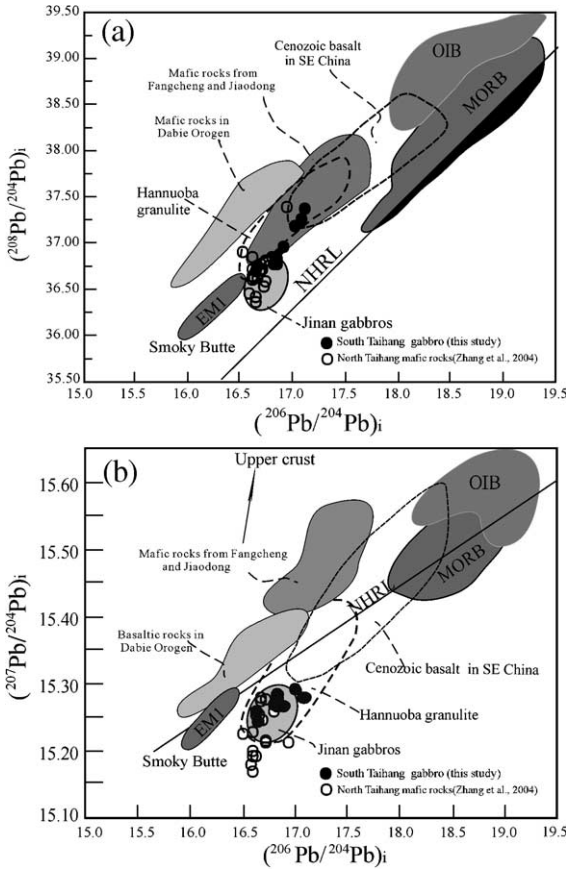

Fig. 8. Initial $^{206}Pb/^{204}Pb$ vs. $^{208}Pb/^{204}Pb$ and $^{207}Pb/^{204}Pb$ (a–b) diagrams for the gabbroic rocks from southern Taihang Mountains. Fields for MORB, OIB and NHRL (north hemisphere reference line) are taken from Hart (1984), and the Smoky Butte lamprophyres from Fraser et al. (1985). Field of lower crust Haonuoba granulites is after Zhou et al. (2002). The Cenozoic basalts in SE China are from Liu et al. (1994) and Zou et al. (2000). Field of early Cretaceous Jinan gabbros is after Zhang et al. (2004), and early Cretaceous volcanics/mafic dikes from Dabie, Jiaodong and Fangcheng after Zhang et al. (2002), Yang et al. (2004), Fan et al. (2001, 2004) and Wang et al. (2005).

DePaolo, 1981) could result in concomitant increase in SiO_2 and $^{87}Sr/^{86}Sr$ and $^{206}Pb/^{204}Pb$, and negative correlation between SiO_2 and $\varepsilon_{Nd}(t)$ and Nb/La (DePaolo, 1981). Such characteristics have not been observed in these gabbroic rocks (Fig. 9a–d and inset in Fig. 7b). The data, together with the high MgO, Ni and Cr contents and lower $^{206}Pb/^{204}Pb$ for these rocks, clearly argue against an AFC process. The scenario of magma mixing is also not favored, because this should generate mixing curves in the isotopic correla-

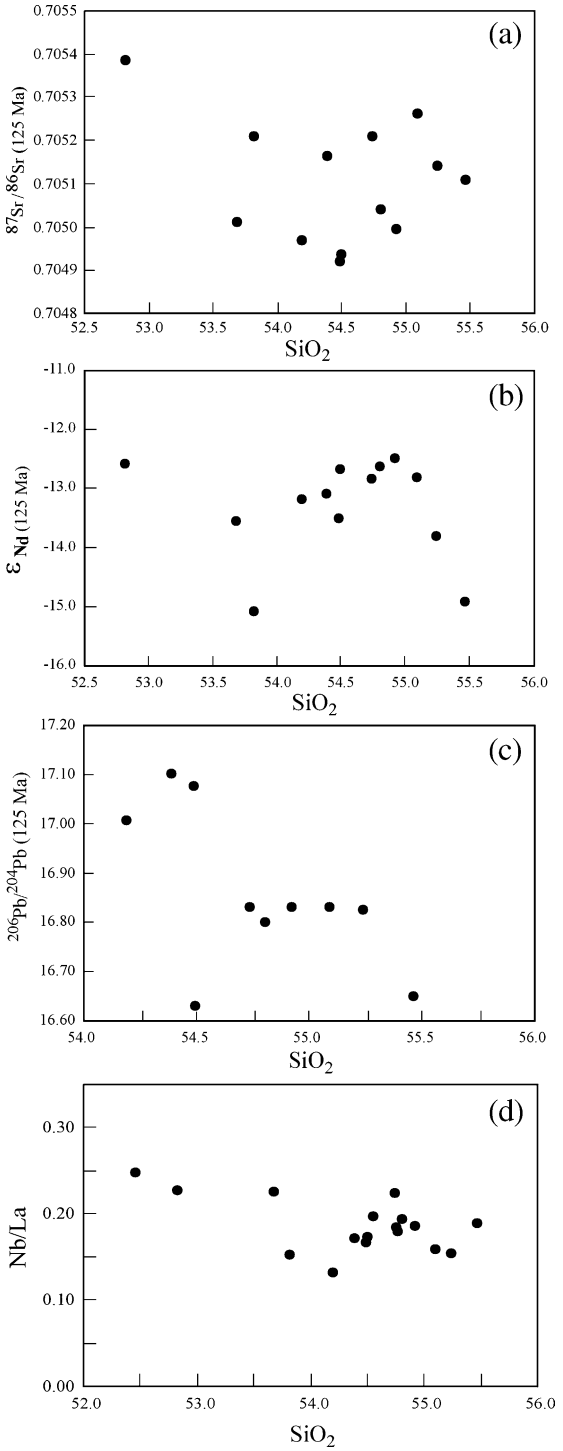

Fig. 9. SiO_2 vs. (a) $^{87}Sr/^{86}Sr(t)$, (b) $\varepsilon_{Nd}(t)$, (c) $^{206}Pb/^{204}Pb$ and (d) Nb/La for the gabbroic rocks from the southern Taihang Mountains.

tion diagrams and on the plots between SiO_2 and isotopic ratios, which are not observed (Figs. 7–9). The normal zoning in plagioclase, amphibole and clinopyroxene (*Background Dataset*) also exclude such a scenario. Therefore the variability of elemental and isotopic compositions in these rocks is more likely an indicative of crustal component involved in their sources.

5.2. Origin of the gabbroic magma

5.2.1. Anatexis of lower crustal granulites or eclogites?

The NCC has an Archean lower crust composed dominantly of garnet granulites (Jahn and Zhang, 1984; Zhou et al., 2002), which is a possible source of the gabbroic magma. However, these gabbroic rocks from the southern Taihang Mountains show the distinct compositions of amphibole from those of the granulites of the NCC, and lower $^{87}Sr/^{86}Sr$ ratios and higher $\varepsilon_{Nd}(t)$ values than those of the lower crust granulite ($^{87}Sr/^{86}Sr=0.7060–0.7200$, $\varepsilon_{Nd}=-32$ to -44; Jahn and Zhang, 1984). Significant Th–U depletion typical in the granulites in the NCC (Zhai et al., 2001) has not been observed in the gabbroic rocks (Fig. 6b). Thus these gabbroic rocks cannot be regarded as the products from the anatexis of the granulites of the NCC. It is also unlikely that they were derived from a young subducted oceanic crust since it is difficult to reconcile with their isotopic data (Figs. 7 and 8). Moreover, no geological evidence supports the subduction of an oceanic crust in the central NCC during the Mesozoic.

Partial melting of eclogites with minor rutiles is a possible mechanism to produce magmas with high LILEs and LREEs and low HFSEs concentrations. However, available experimental studies reveal that partial melts of eclogites are high in SiO_2 (>56%), Al_2O_3 (>17%) and TiO_2 at pressure of <3.0 GPa (~100 km in depth) when the degree of partial melting is less than 50% (Klemme et al., 2002; Rapp et al., 1991), and that there is a decrease in K_2O+Na_2O and an increase in MgO and Al_2O_3 of the partial melts with increasing degree of partial melting (Klemme et al., 2002; Kogiso et al., 2003). This suggests that the Al_2O_3 content in the melt is certainly greater than 17.0% with MgO in a range of 9–11 wt.%, which contrasts with the fact that the gabbroic samples from the southern Taihang Mountains contain low Al_2O_3 (12.4–13.9%) contents. In the plot of Cr vs. Ni (Fig. 10), these rocks have higher Ni contents than the supposed range of boninite and associated mantle-derived melt, similar to the high-mg andesite from Kitakami as the products of melt–peridotite interaction. This also rules out the possibility that the gabbroic rocks in the southern Taihang Mountains were derived from the partial melting of eclogites. Additionally, the eclogitic xenoliths from the pre-existing Archean lower crust, hosted in the Mesozoic intrusions at Xinyang and Xu-Huai in the NCC (Xu et al., 2002a,b; Gao et al., 2004), have Sr–Nd isotopic compositions distinctive from those of the gabbroic rocks in the southern Taihang Mountains (Fig. 6a). Therefore, these rocks should not be originated from granulites and eclogites in the lower continental crust of the NCC, which is also supported by high Ni and mg number of the olivine in the samples (*Background Dataset*).

5.2.2. Melting from hydrated pyroxene-rich refractory peridotite

The high mg number, Ni and Cr and low FeOt and TiO_2 contents suggest a refractory source for these gabbroic rocks that had experienced previous extraction of basaltic melts. High mg numbers in olivine, clinopyroxene and amphibole, and positive correlation between SiO_2 and Al_2O_3 indicate that the primi-

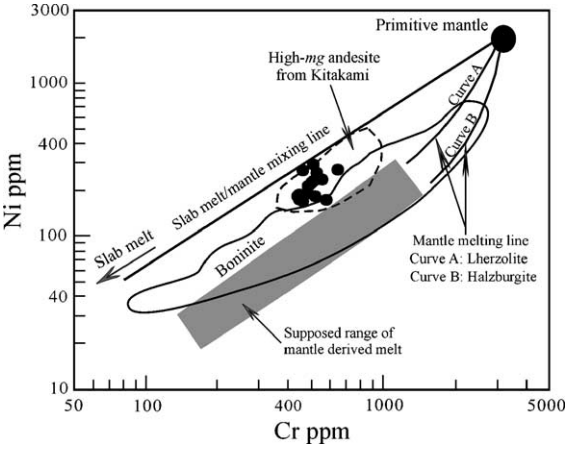

Fig. 10. Plot of Cr and Ni for early Cretaceous gabbroic rocks from the southern Taihang Mountains; the expected range of the mantle-derived melt, boninites and high-mg andesite from Kitakami (Tsuchiya et al., 2005) are also plotted for comparison.

tive magma must have relatively high MgO and low Al_2O_3 contents. Low-Al_2O_3 contents suggest that the source contained high proportion of orthopyroxene or underwent higher degree of melting (Kogiso et al., 1998; Hirose and Kushiro, 1993). However, the high to moderate degree melting products of peridotites generally generate silica-undersaturated magmas enriched in FeO, CaO and TiO_2 (Kogiso et al., 1998). Higher Cr contents (>450 ppm) for these rocks than the Cenozoic basalts from East China derived from pure peridotitic source at comparable MgO of 9–11 wt.% (generally <300 ppm; Liu et al., 1994; Zou et al., 2000) likely indicates the involvement of pyroxenite in their sources. Many high-mg andesites formed by the melting of peridotites previously depleted in clinopyroxene (Kelemen, 1995) Therefore, the lower Al_2O_3 concentrations of these samples likely indicate the existence of higher proportional orthopyroxene in their source.

High-pressure melting experiments show that high-mg melt can be produced by the hydrous or anhydrous refractory peridotite at a smaller degree of melting (Hirose, 1997; Falloon et al., 1988; Baker et al., 1995; Tatsumi, 1981). However, the occurrence of significant amount of biotite and amphibole of these rocks more likely suggests the presence of hydrous phases in the source region, which may facilitate the expansion of olivine volume to trigger the melting of refractory peridotites and produce SiO_2-rich melts (Gallagher and Hawkesworth, 1992; Kushiro, 1972). Although the melting of hydrous peridotites can produce the magmas with high Al_2O_3 and low MgO concentrations, in comparison with those of anhydrous peridotites (Hirose, 1997; Baker et al., 1994), it is more likely that the higher proportional olivine and orthopyroxene in the source resulted in the decreases of Al_2O_3 and CaO and the increases of the SiO_2 and MgO as demonstrated by experimental results (Baker et al., 1994; Hirose and Kushiro, 1993; Kogiso et al., 1998). That is, variations in source compositions significantly affected Al_2O_3, MgO and CaO contents in the partial melts. Consequently, these high-mg melts with higher SiO_2, MgO and lower FeO, Al_2O_3 and CaO contents were likely the melting products of hydrated orthopyroxene-rich refractory peridotite.

The Sr–Nd isotopic systematics for these gabbroic rocks described above indicates that the source might be chronically depleted in Rb but enriched in LREE before partial melting. The extremely low Pb isotopic ratios (Fig. 8a–b) define a trend towards the field for Smoke Butte lamprophyre that was interpreted as the origination from an EMI-like subcontinental lithospheric mantle (Fraser et al., 1985), suggesting the development of an ancient and long-term low U/Pb and Th/Pb source. These characteristics, in combination with obvious depletion in HFSEs and enrichment in LILEs for these rocks, suggest the involvement of an "old" component with a long residence time. Two petrogenetic models can be put forward to explain the contribution to the "old" materials that would be placed within the subcontinental lithosphere: (1) recent involvement of the lower crustal materials and related derivations into the source; (2) ancient metasomatism of carbonatite- or subduction-related fluid/melts derived from the crustal component.

5.2.2.1. Refractory peridotite source recently modified by the lower crustal materials? Lower crustal materials of the NCC can recently be involved into the mantle source by two mechanisms: subduction and delamination (Chen et al., 2004; Gao et al., 2004). However, present data show that the southward subduction of the Mongolo-Okhotsk oceanic plate occurred at the end of the Phanerozoic (Wu et al., 2000; Chen et al., 2000), and the westward subduction of the Pacific Plate under the Asian continent did not occur until ~100 Ma (Engebretson et al., 1985), much younger than the emplacement of the gabbroic rocks in the southern Taihang Mountains. These imply that the involvement of the lower crustal materials in the origin of the gabbroic rocks in the region was related to neither the southward subduction of the Mongolo-Okhotsk oceanic plate nor the westward subduction of the Pacific Plate. On the other hand, if the involvement of the lower crustal materials was associated with the deep subduction/collision between the NCC and Yangtze blocks during the Triassic (e.g., Li et al., 1993), the mantle-derived magma should display "EMII-like" elemental and isotopic systematics characterized by the contemporaneous volcanics/lamprophyres from the southern/eastern margin of the NCC, which are interpreted as derivation from the lithospheric mantle recently contaminated by the lower

crustal materials (e.g., Fangcheng, Yinan, Jiaodong, Dabie areas; Zhang et al., 2002; Xu et al., 2004; Fan et al., 2001, 2004; Wang et al., 2005). However, the gabbroic rocks from the southern Taihang Mountains have an affinity to an EMI-like source, different from that of the contemporaneous volcanics/lamprophyres from the margin of the NCC. It is noted that the southern Taihang Mountains are situated at the center of the NCC, too far away from the subduction zones of the Paleo-Pacific and Mongolo-Okhotsk Plates and Dabie-Sulu Orogen, also arguing against the petrogenetic scenario of the recent involvement of the lower crustal materials into the mantle source by the subduction of the plates.

It is alternative that the lower crust of the NCC was delaminated into the mantle. To test this alternative, we performed a modeling calculation for source mixing in terms of Sr–Nd isotopic composition. The results show that only the source addition of few percents of the lower crustal component (~5%) to the Paleozoic enriched mantle (represented by Ordovician kimberlite-borne peridotites in Mengyin, Zheng and Lu, 1997) or the depleted mantle (Zindler and Hart, 1986) suffices to explain the observed isotopic composition for these gabbroic rocks (curve 3 in Fig. 7a and curve 2 in Fig. 7b). This suggests that the large-scale delamination of the lower crust of the NCC in the southern Taihang Mountains is highly susceptible. Additionally, the direct derivation of the lithospheric mantle hybridized by the proportional lower crust of the NCC should resemble the "normal" basaltic/andesitic rocks rather than high-mg basaltic rocks with high Cr and Ni contents. To produce high-mg andesitic rocks, a petrogenesis model is proposed that the mafic lower crust was foundered into the convecting mantle and subsequently melted and interacted with peridotite. However, the delamination/foundering of the lower crust (even a small volume) should generally be accompanied by the development of voluminous moderate-acid magmatism (especially adakites and associated high-mg andesites), and asthenosphere-/Paleozoic lithospheric mantle-derived magmas due to the uplifting of asthenospheric thermal boundary and revision of the source composition. Such inferred products have been poorly observed in the central NCC (e.g., the southern Taihang Mountains). In contrast, the early Cretaceous mantle-derived magmas extensively occurred in the NCC and have lower $\varepsilon_{Nd}(t)$ values (−6 to −15 in the central NCC and −12 to −24 in the margin of the NCC) than that of Paleozoic lithospheric mantle (Zhang et al., 2002, 2004; Xu et al., 2004; Fan et al., 2001, 2004; Yang et al., 2004). This contradicts the predicted scenario.

5.2.3. *Veined-plus-peridotite previously metasomatised by SiO_2-rich melt?*

In general, the melts from a carbonatitically metasomatised source are highly ultramafic, enriched in K_2O, Na_2O, CaO and FeO, and depleted in Al_2O_3 and SiO_2 (Gasparik and Litvin, 2002; Hammouda, 2003), and have a strong depletion in HFSE relative to REE (LaFlèche et al., 1998). However, these gabbroic rocks are sub-alkaline high-mg basaltic andesites with high $(Hf/Sm)_N$ and low $(Ta/Th)_N$ ratios that plot in the field of subduction-related metasomatism (Fig. 11a). In the TiO_2 vs. FeOt plot (Fig. 11b), all samples fall into the field defined by the experimental melts of refractory peridotite (Falloon et al., 1988), and are also comparable to those of the Italy and Tibetan lamprophyre and Taiwan high-mg andesites (Peccerillo, 1999; Miller et al., 1999; Chung et al., 2001) as origination from the refractory mantle source highly metasomatised by subduction-related melts. Additionally, peridotites metasomatised by carbonatitic melts/fluids are generally characterized by the formation of the secondary clinopyroxene at the expense of the primary orthopyroxene, resulting in high clinopyroxene/orthopyroxene ratios (Kogarko et al., 2001; Yaxley et al., 1998). This is inconsistent with a high proportion of orthopyroxene in the source inferred from these studied rocks. The presence of high proportional orthopyroxene is most likely a consequence of an SiO_2-rich metasomatism in the source, i.e., a reaction of olivine + SiO_2 (metasomatic agent) = orthopyroxene + hornblende (Chalot-Part and Boullier, 1997; Kelemen, 1995).

The fact that the gabbroic rocks in the studied region show significant enrichment in LILEs implies that the source may contain phlogopite (O'Reilly and Griffin, 2000; McInnes et al., 2001). However, partial melting of a phlogopite-bearing source would have generated high-K magma with higher $^{87}Sr/^{86}Sr$ ratios, as shown by the Ordovician Mengyin kimberlites and early Cretaceous Jiaodong lam-

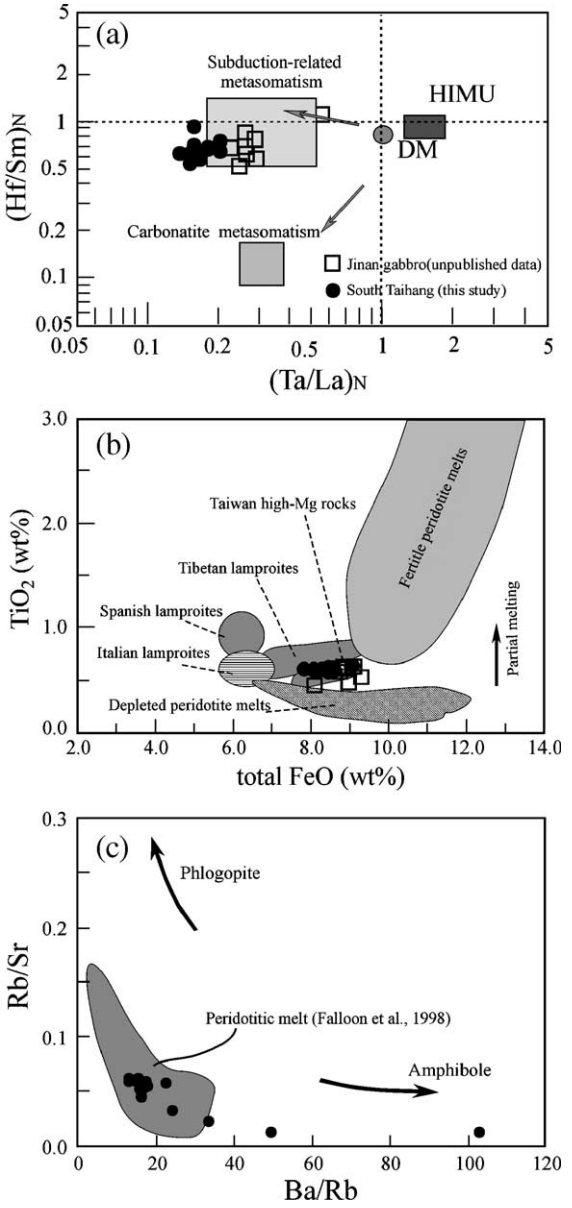

Fig. 11. (a) $(Ta/La)_N$ vs. $(Hf/Sm)_N$ diagram for the gabbroic rocks from the southern Taihang Mountains. The trends of the subduction- and carbonatite-related metasomatism are from LaFlèche et al. (1998); (b) plot of total FeO vs. TiO_2 for the studied gabbroic rocks in comparison with the Italian, Spanish and Tibetan lamprotrites and Taiwan high-mg andesites (Peccerillo, 1999; Miller et al., 1999; Chung et al., 2001), and experimental peridotite melt (Falloon et al., 1988). (c) Rb/Sr vs. Ba/Rb diagram for the gabbroic rocks from the southern Taihang Mountains.

prophyres/volcanics (Zheng and Lu, 1997; Qiu et al., 2002; Yang et al., 2004; Fan et al., 2001; Guo et al., 2001; Xu et al., 2004). Melts from a phlogopite-bearing source are also expected to have high Rb/Sr (>0.1) and low Ba/Rb (<20) ratios, and H_2O/fluid-related metasomatism generally has high Rb/Ba and Rb/Sr ratios (Furman and Graham, 1999). However, these studied gabbroic samples have Ba/Rb=13–50 (except for sample 20HD79) and Rb/Sr=0.01–0.06, suggesting an amphibole-bearing source (Fig. 11c).

Significant Sr and Ba enrichment in these samples (Fig. 6a–b) could be regarded as the evidence for the presence of plagioclase in the source (Jacob et al., 2003), given that significant plagioclase fractionation is discarded. The low HREE abundances observed in these samples (Y<18 ppm, Yb<1.8 ppm) indicate the melting of the source took place within the stability field of garnet. Such geochemical features of the gabbroic rocks are similar to those of adakites and Archean TTG rocks (Defant and Drummond, 1990; Gao et al., 2004; Xu et al., 2002a,b), and may have inherited from the derived SiO_2-rich melt of the recycled gabbroic component in the lower crust that was possibly metamorphosed to eclogitic facies during the subduction (Cooke and O'Brien, 2001; Wang et al., 2004).

Consequently, we here propose that the geochemical features of these gabbroic rocks might be related to an SiO_2-rich metasomatised melt derived from the recycled crustal materials with gabbroic component. These metasomatised melt are characterized by low Sm/Nd and low Rb/Sr ratios, and with time, their source regions would develop low $^{87}Sr/^{86}Sr$ ratios and low $\varepsilon_{Nd}(t)$ values. The crystallized products of the metasomatised melt may have resulted in the development of the amphibole-bearing pyroxenitic veins in the peridotitic wall rocks (Yang et al., 2004; Foley, 1992; Suen and Frey, 1987). These veins favored the major element additions and imparted with the observed elemental and isotopic features. These gabbroic rocks were, therefore, originated from a refractory pyroxenitic vein-plus-peridotite source previously modified by an SiO_2-rich subduction-related melt. This is also evidenced by the presence of metasomatised pyroxenitic xenoliths hosted in the Mesozoic basalts in the central NCC (Xu, 2002; Zhang et al., 2002).

6. Tectonic implications

As described above, it is controversial whether the occurrence of early Cretaceous magmatism in the central NCC (e.g., southern Taihang Mountains) is related to the subduction of the Mongolo-Okhotsk and Pacific oceanic plates (Chen et al., 2004) or the delamination of the lower crustal materials of the NCC (Gao et al., 2004). The modification of the lithospheric mantle related to the deep subduction/collision between the NCC and Yangtze blocks only affected the mantle source beneath the southern/eastern margin of the NCC (Zhang et al., 2002; Xu et al., 2004; Fan et al., 2001, 2004; Wang et al., 2005). A Mesozoic intracontinental tectonic regime in the central NCC is widely accepted. However, the elemental and isotopic systematics of early Cretaceous high-mg gabbroic rocks from the southern Taihang Mountains in the central NCC indicates that the mantle source might have been previously metasomatised by an SiO_2-rich melt derived from the subducted crustal materials. Now the question arises as to when and how such an SiO_2-rich metasomatised melt was generated and involved in the peridotitic source of the central NCC. Here we propose that the Paleoproterozoic subduction/collision between the Eastern and Western Blocks of the NCC along the Central Zone may have played an important role in producing these melts, based on the following considerations.

(1) No evidence is found to support the presence of a Phanerozoic subduction/collision event in the central NCC so far (Gilder et al., 1991; Davis et al., 2001; Zheng et al., 1996). The most important tectonic events prior to the Mesozoic magmatism in the southern Taihang Mountains are the formation of the Eastern and Western Blocks of the NCC during Archean and the subductional and collisional event during Paleoproterozoic (~1850 Ma). The latter led to the amalgamation of the Eastern and Western Blocks (Zhao et al., 2001a, 2005; Zhao, 2001).

(2) A likely explanation for the low $^{206}Pb/^{204}Pb$ and relatively high $^{208}Pb/^{204}Pb$ ratios of the gabbroic rocks in the studied area is that the magma source lost U and had a nearly constant Th/Pb ratio (Eisele et al., 2002; Woodhead and Devey, 1993), which can be easily interpreted by the origination of sediment deposition or subduction involvement (Eisele et al., 2002; Shimoda et al., 2003). The involvement of crustal components during the subduction process might have occurred during the Archean formation of the Eastern and Western Blocks of the NCC or the Paleoproterozoic subduction/collision of these two blocks. It has been suggested that most incompatible elements (e.g., U, Th and Pb) in the crustal components could not recycled into the mantle during Archean due to the higher geothermal gradient and lower solidus temperature of the sediments (Shimoda et al., 2003). Therefore, the younger event (Paleoproterozoic subduction/collision) should be responsible for the origination of the Pb isotopic signature. The simulation results of the three-stage Pb isotope evolution model proposed by Eisele et al. (2002) also show that the recycling time of the crustal components ranges from 1.1 to 1.9 Ga.

(3) The lower crustal materials with proportional gabbroic components have been proposed to be involved into the lithospheric mantle beneath the southern Taihang Mountains during the Paleoproterozoic subduction/collision between the Eastern and Western Blocks of the NCC (Wang et al., 2004).

No matter what tectonic setting, in which the high-mg gabbroic rocks were generated from a refractory hydrated mantle, it is generally believed that a sudden change of the tectonic regime from convergence to extension with a constant high thermal state is essential. Field observations show that regional thrust-fault activation in the region ceased at J_3, and the metamorphic core complexes, extensive volcanism and rifting basins, as the indicative of an extension setting, extensively occurred at K_1 (Davis et al., 2001; Zheng et al., 1996). These suggest that a sudden change from a convergent to extensional regime in the central NCC very likely occurred at ~125 Ma. Xu (2001) emphasized that the thermochemical erosion of the Mesozoic lithosphere in response to the upwelling of the asthenosphere is the dominant cause of the destabilization and thinning of the NCC lithosphere. Zhang et al. (2003) considered that the Triassic subduction/collision

beneath the northern and southern margins of the NCC resulted in the thinning and replacement of the NCC lithosphere. We here consider that Triassic subduction/collision along the northern and southern margins of the NCC may have initiated the cracking and destabilization of the lithosphere beneath the central NCC, but may not have provided sufficient heat to cause the thinning and replacement of the NCC lithosphere The rate of the lithospheric thinning may have suddenly increased till ~125 Ma due to the rapid ascending of the asthenosphere. Consequently, a sudden increase in the rate of lithosphere thinning in response to the rapid asthenosphere upwelling, coupled with the sudden change from a convergent to extensional regime, may be the important mechanism for triggering the melting of the metasomatised lithospheric mantle to generate early Cretaceous high-mg gabbroic rocks in the southern Taihang Mountains.

7. Conclusions

A comprehensive geochronological, mineralogical and geochemical study on the high-mg gabbroic rocks from the southern Taihang Mountains allows us to reach the following conclusions:

(1) The gabbroic rocks were emplaced at ~125 Ma and exhibit high MgO and low Al_2O_3, FeOt and TiO_2 contents, compositionally similar to high-mg basaltic andesites.
(2) These gabbroic rocks are composed of olivine with 78–85% forsterite, magnesio-actinolitic hornblende, diopside–salite and plagioclase with normal An zoning.
(3) They are characterized by a significant enrichment in LILEs and LREE, a depletion in HFSEs and HREEs and "EMI-like" Sr–Nd–Pb isotopic signatures.
(4) Geochemical features of the gabbroic rocks demonstrate that they might have been originated from a refractory pyroxenitic veined-plus-peridotite source previously metasomatised by SiO_2-rich melt. Such melt was probably produced during the Paleoproterozoic subduction/collision between the Eastern and Western Blocks.
(5) The generation of early Cretaceous gabbroic rocks implies a sudden increase in the rate of lithosphere thinning beneath the central NCC in response to the asthenospheric mantle ascending during early Cretaceous.

Acknowledgements

We are grateful to Drs. G.-C. Zhao, Y.-G. Xu and Y.-H. Zhang for their thoughtful discussions and suggestions. We thank S. Foley and two anonymous reviewers for incisive criticisms and helpful suggestions. This study was jointly supported by the Nature Sciences Foundation of China (40303005, 40421303 and 40334039), K.C. Wang Education Foundation, Hong Kong and Chinese Academy of Sciences (GIGCX-03-01).

References

Baker, M.B., Grove, T.L., Price, R., 1994. Primitive basalts and andesites from the Mt. Shasta region, N. California: products of varying melt fraction and water content. Contrib. Mineral Petrol. 118, 111–129.

Baker, M.B., Hirschmann, M.M., Ghlorso, M.S., Stolper, E.M., 1995. Compositions of near-solidus peridotite melts from experiments and thermodynamic calculations. Nature 375, 308–311.

Boyd, F.R., Gurney, J., 1986. Diamonds and African lithosphere. Science 239, 472–477.

Chalot-Part, F., Boullier, A.M., 1997. Metasomatic events in the subcontinental mantle beneath the Eastern Carpathians (Romania): new evidence from trace elements. Contrib. Mineral. Petrol. 129, 284–307.

Chen, B., Zhai, M.G., 2003. Geochemistry of late Mesozoic Lamprophyre dikes from the Taihang Mountains, North China and implications for the subcontinental lithospheric mantle. Geol. Mag. 140 (1), 87–93.

Chen, B., Jahn, B.M., Wilde, S., Xu, B., 2000. Two contrasting Paleozoic magmatic belts in northern Inner Mongolia, China: petrogenesis and tectonic implications. Tectonophysics 328 (1–2), 157–182.

Chen, B., Jahn, B.M., Arakawa, Y., Zhai, M.G., 2004. Petrogenesis of the Mesozoic intrusive complexes from the southern Taihang Orogen, North China Craton: elemental and Sr–Nd–Pb isotopic constraints. Contrib. Mineral. Petrol. 148 (4), 489–501.

Chung, S.L., Wang, K.L., Crawford, A.J., Kamenetsky, V.S., Chen, C.H., Lan, C.Y., Chen, C.H., 2001. High-Mg potassic rocks from Taiwan: implications for the genesis of orogenic potassic lavas. Lithos 59, 153–170.

Compston, W., Williams, I.S., Mayer, C., 1984. U–Pb geochronology of zircons from Lunar Breccia 73217 using a Sensitive

High Resolution Ion Microprobe. Proc. XIV Lunar Planetary Science Conference. J. Geophys. Res. 89, B525–B534 (suppl).

Cooke, R.A., O'Brien, P.J., 2001. Resolving the relationship between high *P–T* rocks and gneisses in collisional terrane: an example from the Gföhl gneiss–granulite association in the Moldanubian Zone, Austria. Lithos 58, 33–54.

Crawford, A.J., Falloon, T.J., Green, D.H., 1989. Classification, petrogenesis and tectonic setting of boninites. In: Crawford, A.J. (Ed.), Boninites and related rocks. Unwin Hyman, London, pp. 1–49.

Cumming, G.L., Richards, J.R., 1975. Ore lead isotope ratios in a continuously changing. Earth Planet. Sci. Lett. 28, 155–171.

Davis, G.A., Zheng, Y.D., Wang, C., Darby, B.J., Zhang, C.H., Gehrels, G., 2001. Mesozoic tectonic evolution of Yanshan fold and thrust belt with emphasis on Hebei and Liaoning Provinces, northern China. In: Hendrix, M.S., Davis, G.A. (Eds.), Paleozoic and Mesozoic Tectonic Evolution of Central Asia: From Continental Assembly to Intracontinental Deformations, Boulder Colorado Geological Society of Am. Memoir., vol. 194, pp. 171–194.

Deer, W.A., Howie, R.A., Zussman, J., 1978. Rock forming minerals. Single-Chain Silicates, vol. 2A. Wiley, New York.

Defant, M.J., Drummond, M.S., 1990. Derivation of some modern arc magmas by melting of young subducted lithosphere. Nature 347, 662–665.

DePaolo, D.J., 1981. Trace element and isotopic effects of combined wall rock assimilation and fractional crystallization. Earth Planet. Sci. Lett. 53, 189–202.

Eisele, J., Sharma, M., Galer, S.J.G., Blicher-Toft, J., Devey, C.W., Hofmann, A.W., 2002. The role of sediment recycling in EMI inferred from Os, Pb, Hf, Nd, Sr isotope and trace element systematics of the Pitcairn hotspot. Earth Planet. Sci. Lett. 196 (3–4), 197–212.

Engebretson, D.C., Cox, A., Gordon, R.G., 1985. Relative motions between oceanic and continental plates in the Pacific basins. Spec. Pap.-Geol. Soc. Am. 206, 1–59.

Falloon, T.J., Green, D.H., Hatton, C.J., Harris, K.L., 1988. Anhydrous partial melting of a fertile and depleted peridotite from 2 to 30 kbar and applications to basalt petrogenesis. J. Petrol. 29, 1257–1282.

Fan, W.M., Zhang, H.F., Baker, J., Jarvis, K.E., Mason, P.R.D., Menzies, M.A., 2000. On and off the North China Craton: where is the Archean keel? J. Petrol. 41 (7), 933–950.

Fan, W.M., Guo, F., Wang, Y.J., 2001. Post-orogenic bimodal volcanism along the Sulu Orogenic belt in eastern China. Phys. Chem. Earth (A) 26 (9–10), 733–746.

Fan, W.M., Guo, F., Wang, Y.J., Zhang, M., 2004. Late Mesozoic volcanism in the northern Huaiyang tectono-magmatic belt, central China: Partial melts from a lithospheric mantle with subducted continental crust relicts beneath the Dabie Orogen? Chem. Geol. 209 (1–2), 27–48.

Foley, S.F., 1992. Vein-plus-wall rock melting mechanisms in the lithosphere and the origin of potassic alkaline magmas. Lithos 28, 435–453.

Fraser, K.J., Hawkesworth, C.J., Erland, A.J., Mitchell, R.H., Scott-Smith, B.H., 1985. Sr–Nd–Pb isotopic and minor element geochemistry of lamprophyres and kimberlites. Earth Planet. Sci. Lett. 76, 57–70.

Furman, T., Graham, D., 1999. Erosion of lithospheric mantle beneath the East African Rift system: geochemical evidence from the Kivu volcanic province. Lithos 48 (1–4), 237–262.

Gallagher, K., Hawkesworth, C.J., 1992. Dehydration melting and the generation of continental flood basalts. Nature 358, 57–59.

Gao, S., Luo, T.C., Zhang, B.R., Zhang, H.F., Han, Y.W., Zhao, Z.D., Hu, Y.K., 1998. Chemical composition of the continental crust as revealed by studies in East China. Geochim. Cosmochim. Acta 62, 1959–1975.

Gao, S., Lin, W.L., Qiu, Y.M., 1999. Contrasting geochemical and Sm–Nd isotopic compositions of Achaean metasediments from the Kongling high-grade terrain of the Yangtze Craton: evidence for cratonic evolution and redistribution of REE during crustal anatexis. Geochim. Cosmochim. Acta 63 (13/14), 2071–2088.

Gao, S., Rudnick, R.L., Yuan, H.L., Liu, X.M., Liu, Y.S., Xu, W.L., Ling, W.L., Ayers, J., Wang, X.C., Wang, Q.H., 2004. Recycling lower continental crust in the North China craton. Nature 432 (16), 892–897.

Gasparik, T., Litvin, Y.A., 2002. Experimental investigation of the effect of metasomatism by carbonatic melt on the composition and structure of the deep mantle. Lithos 60 (3–4), 129–143.

Gilder, S.A., Keller, G.R., Luo, M., Goodell, P.C., 1991. Eastern Asia and the western Pacific: timing and spatial distribution of rifting in China. Tectonophysics 197, 225–243.

Griffin, W.L., O'Reilly, S.Y., Ryan, C.G., 1992. Composition and thermal structure of the lithosphere beneath South African, Siberia and China: proton microprobe studies. Inter'l Symp Cenozoic Volcanic Rocks and Deep-seated Xenoliths in China and its Environs, pp. 65–66. Beijing (Abstract).

Guo, F., Fan, W.M., Wang, Y.J., 2001. Late-Mesozoic mafic intrusive complexes in north china block: constraints on the nature of subcontinental lithospheric mantle. Phys. Chem. Earth (A) 26 (9–10), 759–771.

Hammouda, T., 2003. High-pressure melting of carbonated eclogite and experimental constraints on carbon recycling and storage in the mantle. Earth Planet. Sci. Lett. 214, 357–368.

Hart, S.R., 1984. A large-scale isotopic anomaly in the Southern Hemisphere mantle. Nature 309, 753–757.

HBGMR (Regional geology of Beijing, Tianjin and Heibei Province), 1989. Geol. Pub. House, Beijing 50-241 (in Chinese).

Hirose, K., 1997. Melting experiments on KLB-1 under hydrous conditions and generation of high-magnesia andesitic melts. Geology 25, 42–44.

Hirose, K., Kushiro, I., 1993. Partial melting of dry peridotites at high pressures: determination of compositions of melts segregated from peridotite using aggregates of diamond. Earth Planet. Sci. Lett. 114, 477–489.

Jacob, D.E., Schmickler, B., Schulze, D.J., 2003. Trace element geochemistry of coesite-bearing eclogites from the Roberts Victor kimberlite Kaapvaal craton. Lithos 71 (2–4), 337–351.

Jahn, B.M., Zhang, Z.Q., 1984. Archean granulite gneisses from eastern Hebei Province, China: rare earth geochemistry and tectonic implications. Contrib. Mineral. Petrol. 85, 224–243.

Jahn, B.M., Wu, F.Y., Lo, C.H., 1999. Crust–mantle interaction induced by deep subduction of the continental crust: geochemical and Sr–Nd isotopic evidence from post-collisional mafic–ultramafic intrusions of the northern Dabie Complex, Central China. Chem. Geol. 157, 119–146.

Kelemen, P.B., 1995. Genesis of high-ma andesite and the continental crust. Contrib. Mineral. Petrol. 120, 1–19.

Klemme, S., Blundy, J.D., Wood, B.J., 2002. Experimental constraints on major and trace element partitioning during partial melting of eclogite. Geochim. Cosmochim. Acta 66 (17), 3109–3123.

Kogarko, L.N., Kurat, G., Ntaflos, T., 2001. Carbonatite metasomatism of the oceanic mantle beneath Fermando de Noronha Island, Brazil. Contrib. Mineral Petrol. 140, 577–587.

Kogiso, T., Hirose, K., Takahashi, E., 1998. Melting experiments on homogeneous mixtures of peridotite and basalt: application to the genesis of ocean island basalts. Earth Planet. Sci. Lett. 162, 45–61.

Kogiso, T., Hirschmann, M.M., Frost, D.J., 2003. High-pressure partial melting of garnet pyroxenite: possible mafic lithologies in the source of ocean island basalts. Earth Planet. Sci. Lett. 216, 603–617.

Kushiro, I., 1972. Effect of water on the composition of magmas formed at high pressure. J. Petrol. 13, 311–344.

LaFlèche, M.R., Camire, G., Jenner, G.A., 1998. Geochemistry of post-Acadian, Carboniferous continental intraplate basalts from the Maritimes Basin, Magdalen islands, Quebec, Canada. Chem. Geol. 148, 115–136.

Leake, B.E., 1978. Nomenclature of amphiboles. Am. Mineral. 63, 1023–1052.

Li, S.G., Xiao, Y.L., Liou, D.L., 1993. Collision of the North China and Yangtze blocks and formation of coesite-bearing eclogites: timing and process. Chem. Geol. 109, 89–111.

Liu, D.Y., Nutman, A.P., Compston, W., Wu, J.S., Shen, Q.H., 1991. Remnants of 3800 Ma crust in the Chinese part of the Sino-Korean craton. Geology 20, 339–342.

Liu, C.Q., Masuda, A., Xie, G.H., 1994. Major- and trace element compositions of Cenozoic basalts in eastern China: petrogenesis and mantle source. Chem. Geol. 111, 19–42.

Ludwig, K.R., 2001a. Squid 1.02. A user manual. Berkeley Geochronological Center Special, Berkeley, pp. 1–219.

Ludwig, K.R., 2001b. Using Isoplot/EX, version 2.49. A Geochronological Toolkit for Microsoft Excel. Berkeley Geochronological Center Special Publiction, Berkeley, pp. 1–55.

McCarron, J.J., Smellie, J.L, 1998. Tectonic implications of fore-arc magmatism and generation of high-magnesian andesites: Alexander Island, Antarctica. J. Geol. Soc. Lond. 155, 269–280.

McInnes, B.I.A., Gregoire, M., Binns, R.A., Herzig, P.M., Hannington, M.D., 2001. Hydrous metasomatism of oceanic sub-arc mantle, Lihir, Papua New Guinea: petrology and geochemistry of fluid-metasomatised mantle wedge xenoliths. Earth Planet. Sci. Lett. 188 (1–2), 169–183.

McLennan, S.M., Taylor, S.R., McCulloch, M.T., Maynard, J.B., 1990. Geochemical and Nd–Sr isotopic composition of deep sea turbidites. Geochim. Cosmochim. Acta. 54, 2015–2050.

Menzies, M.A., Xu, Y.G., 1998. Geodynamics of the North China Craton. In: Flower, M.F.J., Chung, S.L., Lo, C.H., Lee, T.Y. (Eds.), Mantle dynamics and plate interaction in East Asia, American Geophysics Union, Geodynamics Series, vol. 27, pp. 155–165.

Miller, C., Schuster, R., Klotzli, U., Frank, W., Purtsgheller, F., 1999. Post-collisional potassic and ultrapotassic magmatism in SW Tibet: geochemical and Sr–Nd–Pb–O isotopic constraints for mantle source characteristics and petrogenesis. J. Petrol. 40, 1399–1424.

Nelson, D.R., 1997. Evolution of the Archaean granite–greenstone terranes of the Eastern Goldfields, Western Australia: SHRIMP U–Pb zircon constraints. Precambrian Res. 83 (1–3), 57–81.

O'Reilly, S., Griffin, W.L., 2000. Apatite in the mantle: implications for metasomatic processes and high heat production in Phanerozoic mantle. Lithos 53, 217–232.

Peccerillo, A., 1999. Multiple mantle metasomatism in central-southern Italy: geochemical effects, timing and geodynamic implications. Geology 27, 315–318.

Peng, T.P., Wang, Y.J., Fan, W.M., Peng, B.X., Guo, F., 2004. SHRIMP zircon U–Pb geochronology of the diorites for the southern Taihang Mountains in Central North China and its petrogenesis. Acta Petrologica Sin. 20 (5), 1253–1262 (in Chinese with English abstract).

Qi, L., Hu, J., Greggoire, C., 2000. Determination of trace elements in granites by inductively coupled plasma mass spectrometry. Talanta 51, 507–513.

Qiu, J.S., Xu, X.S., Lo, Q.H., 2002. Potassium-rich volcanic rocks and lamprophyres in western Shandong Province: $^{40}Ar/^{39}Ar$ dating and source tracing. Chin. Sci. Bull. 4 (2), 91–99.

Rapp, R.P., Watson, E.B., Miller, C.F., 1991. Partial melting of amphibolite/eclogite and the origin of Archean trondhjemites and tonalites. Precambrian Res. 51, 1–25.

Rudnick, R.L., Fountain, D.M., 1995. Nature and composition of the continental crust: a lower crustal perspective. Rev. Geophys. 33, 267–309.

Schmidt, M.W., 1992. Amphibole composition in tonalite as a function of pressure: An experimental calibration of the Al-in-hornblende barometer. Contrib. Mineral Petrol. 110, 304–310.

Shimoda, G., Tatsumi, Y., Morishita, Y., 2003. Behavior of subducting sediments beneath an arc under high geothermal gradient: constraints from the Miocene SW Japan arc. Geochem. J. 37, 503–518.

Steiger, R.H., Jäger, E., 1977. Subcommission on geochronology; convection on the use of decay constants in geochronology and cosmochronology. Earth Planet. Sci. Lett. 36, 359–362.

Suen, C.J., Frey, F.A., 1987. Origins of the mafic and ultramafic rocks in the Ronda peridotite. Earth Planet. Sci. Lett. 85 (1–3), 183–202.

Sun, X.Y., Hong, Z.Y., 1999. Minor element geochemistry of Mesozoic magmatic intrusions of southern Taihang Mountains. J. Geol. Mineral. Resour. North China 14 (1), 1–17.

Sun, S.S., McDonough, W.F., 1989. Chemical and isotopic systematics of oceanic basalts: implication for mantle composition and processes. In: Sauders, A.D., Norry, M.J. (Eds.), Magmatism in the Ocean Basins, Special Publication-Geological Society of London, vol. 42, pp. 313–345.

Tan, D.J., Lin, J.Q., 1994. Mesozoic potassic rocks in the North China. Seism Pub House, Beijing, 1-184 (in Chinese).

Tatsumi, Y., 1981. Melting experiments on a high-magnesian andesite. Earth Planet. Sci. Lett. 60, 305–317.

Taylor, S.R., McLennan, S.M., 1985. The continental crust: Its composition and evolution. Oxford Press Blackwell, pp. 1–312.

Tsuchiya, T., Suzuki, S., Kimura, J.I., Kagami, H., 2005. Evidence for slab melt/mantle reaction: petrogenesis of early Cretaceous and Eocene high-Mg andesites from the Kitakami Mountains, Japan. Lithos 79, 179–206.

Wang, Y.J., Fan, W.M., Zhang, Y.H., Guo, F., 2003. Structural evolution and $^{40}Ar/^{39}Ar$ dating of the Zanhuang metamorphic domain in the North China Craton: constraints on Paleoproterozoic tectonothermal overprinting. Precambrian Res. 122/1–4, 159–182.

Wang, Y.J., Fan, W.M., Zhang, Y.H., 2004. Geochemical, $^{40}Ar/^{39}Ar$ geochronological and Sr–Nd isotopic constraints on the origin of Paleoproterozoic mafic dikes from the southern Taihang Mountains and implications for the ca. 1800 Ma event of the North China Craton. Precambrian Res. 135 (1–2), 55–79.

Wang, Y.J., Fan, W.M., Zhang, H.F., Peng, T.P., Guo, F., 2005. Nature of the Mesozoic lithospheric mantle and tectonic decoupling beneath the Dabie Orogen, Central China: evidence from $^{40}Ar/^{39}Ar$ geochronology, elemental and Sr–Nd–Pb isotopic compositions of Mesozoic mafic rocks. Chem. Geol. 220, 165–189.

Woodhead, J.D., Devey, C.W., 1993. Geochemistry of the Pitcairn Seamounts: I. Source character and temporal trends. Earth Planet. Sci. Lett. 116, 81–99.

Wu, F.Y., Jahn, B.M., Wilde, S., Sun, D.Y., 2000. Phanerozoic crustal growth: U–Pb and Sr–Nd isotopic evidence from the granites in northeastern China. Tectonophysics 328 (1–2), 89–113.

Xu, Y.G., 2001. Thermo-tectonic destruction of the Achaean lithospheric keel beneath the Sino-Korean Craton in China: evidence timing and mechanism. Phys. Chem. Earth (A) 26 (9–10), 47–757.

Xu, Y.G., 2002. Evidence for crustal components in the mantle and constraints on crustal recycling mechanism: pyrexonite xenoliths from Hannuoba, North China. Chem. Geol. 182, 301–322.

Xu, J.F., Shinjo, R., Defant, M.J., Wang, Q., Rapp, R.P., 2002. Origin of Mesozoic adakitic intrusive rocks in the Ningzhen area of east China: partial melting of delaminated lower continental crust? Geology 30, 1111–1114.

Xu, W.L., Wang, D.Y., Liu, X.C., Wang, Q.H., Lin, J.Q., 2002. Discovery of eclogite inclusions and its geological significance in early Jurassic intrusive complex in Xuzhou, northern Anhui, eastern China. Chin. Sci. Bull. 47, 1212–1216.

Xu, Y.G., Ma, J.L., Huang, X.L., Iizuka, Y., Chung, S.L., Wang, Y.B., Wu, X.Y., 2004. Early Cretaceous gabbroic complex from Yinan, Shandong Province: petrogenesis and mantle domains beneath the North China Craton. Int. J. Earth Sci. 93, 1025–1041.

Yang, J.H., Chung, S.L., Zhai, M.G., Zhou, X.H., 2004. Geochemical and Sr–Nd–Pb isotopic compositions of mafic dikes from the Jiaodong Peninsula, China: Evidence for vein-plus-peridotite melting in the lithospheric mantle. Lithos 73, 145–160.

Yaxley, G.M., Green, D.H., Kamenetsky, V., 1998. Carbonatite metasomatism in the southeastern Australian lithosphere. J. Petrol. 39, 1917–1930.

Zhai, M.G., Guo, J.H., Liu, W.J., 2001. An exposed cross-section of early Precambrian continental lower crust in the North China Craton. Phys. Chem. Earth, Part A Solid Earth Geod. 26 (9–10), 781–792.

Zhang, B.R., Luo, T.C., Gao, S., Ouyang, J.P., Chen, D.X., Ma, Z.D., Han, Y.W., Gu, X.M., 1994. Geochemical study of the lithosphere, tectonism and metallogenesis in the Qinling-Dabashan region. Press China Univ Geosci, Wuhan, pp. 1–446.

Zhang, H.F., Sun, M., Zhou, X.H., Fan, W.M., Zhai, M.G., Yin, J.F., 2002. Mesozoic lithosphere destruction beneath the North China Craton: evidence from major, trace element, and Sr–Nd–Pb isotope studies of Fangcheng basalts. Contrib. Mineral. Petrol. 141, 241–253.

Zhang, H.F., Sun, M., Zhou, X.H., Zhou, M.F., Fan, W.M., Zheng, J.P., 2003. Secular evolution of the lithosphere beneath the eastern North China Craton: evidence from Mesozoic basalts and high-mg andesites. Geochim. Cosmochim. Acta 67 (22), 4373–4387.

Zhang, H.F., Sun, M., Zhou, M.F., Fan, W.M., Zhou, X.H., Zhai, M.G., 2004. Highly heterogeneous late Mesozoic lithospheric mantle beneath the North China Craton: evidence from Sr–Nd–Pb isotopic systematics of mantle igneous rocks. Geol. Mag. 141, 55–62.

Zhao, G.C., 2001. Paleoproterozoic assembly of the North China Craton. Geol. Mag. 138, 87–91.

Zhao, G.C., Cawood, P.A., Lu, L.Z., 1999. Petrology and *P–T* history of the Wutai amphibolites: implications for tectonic evolution of the Wutai Complex, China. Precambrian Res. 93, 181–199.

Zhao, G.C., Cawood, P.A., Wilde, S.A., Lu, L.Z., 2000. Metamorphism of basement rocks in the Central Zone of the North China Craton: implications for Paleoproterozoic tectonic evolution. Precambrian Res. 103, 55–88.

Zhao, G.C., Wilde, S.A., Cawood, P.A., Sun, M., 2001. Archean blocks and their boundaries in the North China Craton: lithological, geochemical, structural and *P–T* path constraints and tectonic evolution. Precambrian Res. 107, 45–73.

Zhao, G.C., Cawood, P.A., Wilde, S.A., 2001. High-pressure granulites (retrograded eclogites) from the Hengshan complex, North China Craton: petrology and tectonic implications. J. Petrol. 42, 1141–1170.

Zhao, G.C., Sun, M., Wilde, S.A., Li, S.Z., 2005. Late Archean to Paleoproterozoic evolution of the North China Craton: key issues revisited. Precambrian Res. 136, 177–202.

Zheng, J.P., Lu, X.F., 1997. A study on the Sr–Nd isotopic compositions of mantle xenoliths bearing in kimberlites in eastern China. Earth Science 18(sup), 15–17 (in Chinese with English abstract).

Zheng, Y.Z., Zhang, Q., Wang, Y., Liu, R., Wang, S.G., Zuo, G., Wang, S.Z., Lkaasuren, B., Badarch, G., Badamgarav, Z., 1996. Great Jurassic thrust sheets in Beishan (North Mountains)-Gobi area of China and southern Mongolia. J. Struct. Geol. 18, 1111–1126.

Zhou, X.H., Sun, M., Zhang, G.H., Chen, S.H., 2002. Continental crust and lithospheric mantle interaction beneath North China: isotopic evidence from granulite xenoliths in Hannuoba, Sino-Korean Craton. Lithos 62, 111–124.

Zindler, A., Hart, S.R., 1986. Chemical geodynamics. Annu. Rev. Earth Planet. Sci. 14, 493–571.

Zou, H.B., Zindler, A., Xu, X.S., 2000. Major, trace element, and Nd, Sr and Pb studies of Cenozoic basalts in SE China: mantle sources, regional variations and tectonic significance. Chem. Geol. 171, 33–47.